Article

Molecular Cell

Translational Control through Differential Ribosome Pausing during Amino Acid Limitation in Mammalian Cells

Graphical Abstract

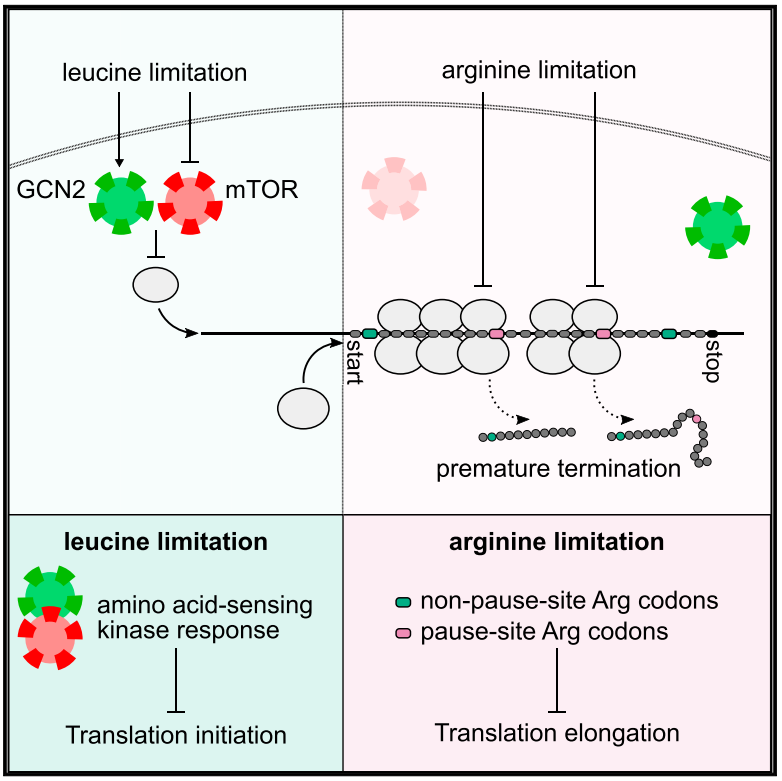

Authors

Alicia M. Darnell, Arvind R. Subramaniam, Erin K. O'Shea

Correspondence

rasi@fredhutch.org (A.R.S.), osheae@hhmi.org (E.K.O.)

In Brief

The mTORC1 and GCN2 signaling pathways sense amino acid deprivation in mammalian cells. Darnell et al. find that when these pathways do not optimally regulate translation upon deprivation of an amino acid, ribosome pausing at a subset of its codons emerges as a regulatory mechanism to selectively reduce protein expression.

Highlights

- Ribosomes pause at only a subset of codons upon arginine but not leucine limitation
- Selective ribosome pausing is driven by loss of charging of corresponding tRNAs
- mTORC1/GCN2 signaling responses determine the magnitude of ribosome pausing
- Ribosome pausing reduces protein synthesis rate and causes premature termination

Darnell et al., 2018, Molecular Cell *71*, 229–243
July 19, 2018
https://doi.org/10.1016/j.molcel.2018.06.041

CellPress

Molecular Cell
Article

Translational Control through Differential Ribosome Pausing during Amino Acid Limitation in Mammalian Cells

Alicia M. Darnell,[1] Arvind R. Subramaniam,[2,5,*] and Erin K. O'Shea[1,3,4,*]
[1]Department of Molecular and Cellular Biology, Harvard University, Cambridge, MA 02138, USA
[2]Basic Sciences Division and Computational Biology Program of Public Health Sciences Division, Fred Hutchinson Cancer Research Center, Seattle, WA 98109, USA
[3]Howard Hughes Medical Institute
[4]Department of Chemistry and Chemical Biology and Faculty of Arts and Sciences Center for Systems Biology Harvard University, Cambridge, MA 02138, USA
[5]Lead Contact
*Correspondence: rasi@fredhutch.org (A.R.S.), osheae@hhmi.org (E.K.O.)
https://doi.org/10.1016/j.molcel.2018.06.041

SUMMARY

Limitation for amino acids is thought to regulate translation in mammalian cells primarily by signaling through the kinases mTORC1 and GCN2. We find that a selective loss of arginine tRNA charging during limitation for arginine regulates translation through ribosome pausing at two of six arginine codons. Surprisingly, limitation for leucine, an essential and abundant amino acid in protein, results in little or no ribosome pausing. Chemical and genetic perturbation of mTORC1 and GCN2 signaling revealed that their robust response to leucine limitation prevents ribosome pausing, while an insufficient response to arginine limitation leads to loss of tRNA charging and ribosome pausing. Ribosome pausing decreases protein production and triggers premature ribosome termination without reducing mRNA levels. Together, our results suggest that amino acids that are not optimally sensed by the mTORC1 and GCN2 pathways still regulate translation through an evolutionarily conserved mechanism based on codon-specific ribosome pausing.

INTRODUCTION

Protein synthesis consumes the highest fraction energy stores and metabolites for biomass production in proliferating cells (Buttgereit and Brand, 1995; Hosios et al., 2016) and is thus tightly controlled in response to the levels of its amino acid substrates. In eukaryotic cells, amino acid limitation is sensed by two conserved signaling pathways anchored by the kinases mechanistic target of rapamycin in complex 1 (mTORC1) and general control nonderepressible 2 (GCN2) (Kimball, 2002). Amino acid limitation inhibits mTORC1 signaling and activates GCN2 signaling, both of which reduce overall protein synthesis through a decrease in the rate of ribosome initiation on mRNA transcripts (Sonenberg and Hinnebusch, 2009). The failure of either pathway to respond to amino acid limitation can lead to cell death, particularly in nutrient-poor contexts like tumors (Nofal et al., 2017; Ye et al., 2010), underscoring the importance of regulatory control over protein synthesis in maintaining cellular homeostasis.

Although the mTORC1 and GCN2 pathways respond strongly to simultaneous limitation for all 20 amino acids (Kimball, 2002), their responses to individual amino acid limitation diverge. mTORC1 signaling is highly sensitive to leucine levels and, to a lesser extent, arginine and glutamine levels (Hara et al., 1998). GCN2 is activated by binding a wide range of uncharged tRNAs (Dong et al., 2000; Zaborske et al., 2010), but its downstream effectors vary in their responses to individual amino acids (Jousse et al., 2000; Tang et al., 2015). As many cancers exhibit dependence on specific amino acids (Vander Heiden and DeBerardinis, 2017), it is crucial to understand how these variegated mTORC1 and GCN2 responses are integrated, and whether they are sufficient, to regulate protein synthesis upon individual amino acid limitation.

Amino acid limitation can also affect protein synthesis by reducing the elongation rate of ribosomes. In bacteria, limitation for auxotrophic amino acids causes loss of tRNA charging and ribosome pausing at a subset of cognate synonymous codons (Dittmar et al., 2005; Subramaniam et al., 2013a), resulting in abortive termination and a consequent decrease in protein expression (Ferrin and Subramaniam, 2017; Subramaniam et al., 2013b, 2014).

Ribosome pausing has been observed in pathological mammalian states, including a mouse model of neurodegeneration (Ishimura et al., 2014), and human tumor samples (Loayza-Puch et al., 2016), although the cause of steady-state pausing remains unclear. Further, the codon specificity and effect of ribosome pausing on protein expression have not been studied in mammalian cells, though codon usage frequency and tRNA levels have been implicated in the regulation of ribosome elongation rate and protein production during metastasis, differentiation, and amino acid limitation (Gingold et al., 2014; Goodarzi et al., 2016; Saikia et al., 2016). However, ribosome profiling

studies have failed to find a simple relationship between codon usage, tRNA levels, and ribosome elongation in mammalian cells (Ingolia et al., 2011; Qian et al., 2012).

Here, we investigated how amino acid signaling pathways and codon usage interact to regulate protein synthesis in response to limitation for single amino acids across multiple human cell lines. We focused on two amino acids, leucine and arginine, which can both regulate protein synthesis by acting as direct signals to mTORC1 (Chantranupong et al., 2016; Wang et al., 2015; Wolfson et al., 2016). We establish a molecular framework relating tRNA charging, ribosome elongation, and protein expression during amino acid limitation, and thus our work provides a rational starting point from which to dissect disease states, such as cancers, that experience nutrient limitation and dysregulated ribosome dynamics.

RESULTS

Ribosomes Pause at Specific Synonymous Codons upon Limitation for Arginine but Not Leucine

To systematically explore the effect of individual amino acid depletion on translation in mammalian cells, we performed ribosome profiling (Ingolia et al., 2009, 2012) in three human cell lines (HEK293T, HeLa, and HCT116) during limitation for either leucine or arginine. Although ribonuclease I (RNaseI) is typically used to generate RNA footprints for ribosome profiling, micrococcal nuclease (MNase) better preserved monosome integrity (Figures S1A–S1C; STAR Methods), and sequencing the resulting footprints (Figure S1D) yielded reads with 3 nt periodicity enriched in coding regions, despite a broader length distribution (Dunn et al., 2013; Reid et al., 2015) (Figures S1E–S1G). To assess the extent of ribosome pausing upon amino acid limitation, we quantified the net increase in normalized average ribosome footprint density in the window around each of the 61 sense codons (Figures 1A and S1H; STAR Methods).

Upon arginine limitation for 3 hr, two of the six arginine codons (CGC and CGU) had a substantial increase in ribosome density across all three cell lines (Figures 1A–1C, and S1H). Ribosome pausing at these codons increased after arginine limitation for 6 hr (Figure 1B). None of the codons encoding the other 19 amino acids had increased ribosome density upon arginine limitation (Figures 1A and S1H). We also observed smaller peaks in ribosome density approximately one ribosome footprint length (~30 nt) behind the major peaks at CGC and CGU codons (Figures 1B and 1C, asterisks). Similar satellite peaks, presumably caused by collision of the trailing ribosome with the paused ribosome, have been previously observed during limitation for single amino acids in *E. coli* (Subramaniam et al., 2014) and *S. cerevisiae* (Guydosh and Green, 2014).

In contrast, none of the six leucine codons displayed a consistent increase in ribosome density in response to leucine limitation (Figures 1A–1C and S1H). Since leucine cannot be synthesized, we were surprised to find that elongation at leucine codons was largely unperturbed. We considered the possibility that cells do not experience major changes in intracellular leucine levels upon its external limitation. However, intracellular arginine and leucine levels fell close to the detection limit of our measurement when they were each removed from the medium, suggesting that these cells are effectively amino acid starved (Figure S1I).

We then tested whether the increase in ribosome density at specific codons upon arginine limitation correlated with simple measures of codon optimality or tRNA abundance, as hypothesized previously (Gingold et al., 2014; Goodarzi et al., 2016; Saikia et al., 2016). The extent of pausing at a codon did not correlate significantly in any cell line with either transcriptomic codon usage (Figures 1D and S1J) or genomic copy number of the cognate tRNA (Figures 1E, S1K, and S1L; Spearman's rank coefficient p values > 0.05). Nevertheless, the consistent hierarchy of codon-specific ribosome pausing upon arginine limitation and its absence during leucine limitation suggested a common underlying principle.

Selective Loss of tRNA Charging upon Amino Acid Limitation Sets the Hierarchy of Ribosome Pausing at Synonymous Codons

Because the ribosome elongation rate at a codon depends on recruitment of the cognate charged tRNA, the arginine tRNA that decodes the pause-site codons CGC and CGU, with the anticodon ACG ($tRNA^{Arg}_{ACG}$), should exhibit a greater charging loss upon arginine limitation than the isoacceptor tRNAs that decode the remaining four arginine codons. In line with this expectation, $tRNA^{Arg}_{ACG}$ lost 70% of its charging upon arginine limitation in HEK293T cells (Figures 2A, 2B, and S2A). By contrast, $tRNA^{Arg}_{CCG}$ and $tRNA^{Arg}_{UCG}$, which decode the arginine codons CGG and CGA at which we did not observe pausing, lost less than 45% of their charging (Figures 2A, 2B, and S2A). All leucine tRNAs tested lost less than 40% of their charging upon leucine limitation, consistent with the observation that there is no ribosome pausing at leucine codons (Figures 2A, 2C, and S2B). Charging loss was also more severe for $tRNA^{Arg}_{ACG}$ than a leucine tRNA in the HCT116 cell line (Figure S2C). As expected, arginine and leucine tRNAs were between 75% and 90% charged during growth in rich conditions or upon limitation for a non-cognate amino acid (Figures 2A–2C, and S2A–S2C). Overall, we found a positive correlation between the change in ribosome density at a codon and the loss in charging of the decoding tRNA upon limitation for the cognate amino acid (Figure 2D; Spearman's rank coefficient p value = 0.015), suggesting that tRNA charging loss underlies ribosome pausing.

Differential mTORC1 and GCN2 Responses to Arginine and Leucine Limitation

We next examined whether the emergence of ribosome pausing during arginine but not leucine limitation might be related to the amino acid signaling response through the GCN2 and mTORC1 kinases, since they are presumed to sense amino acid levels and coordinately regulate protein synthesis in order to maintain intracellular amino acid homeostasis (Park et al., 2017; Zhang et al., 2002). Consistent with previous reports (Hara et al., 1998), we observed greater mTORC1 inhibition during limitation for leucine in comparison to arginine; levels of the mTORC1 target phosphorylated ribosomal protein S6 kinase 1 (P~S6K) fell by 75% during leucine limitation and only 45% during arginine limitation in HEK293T cells (Figure 3A). Levels of the S6K target

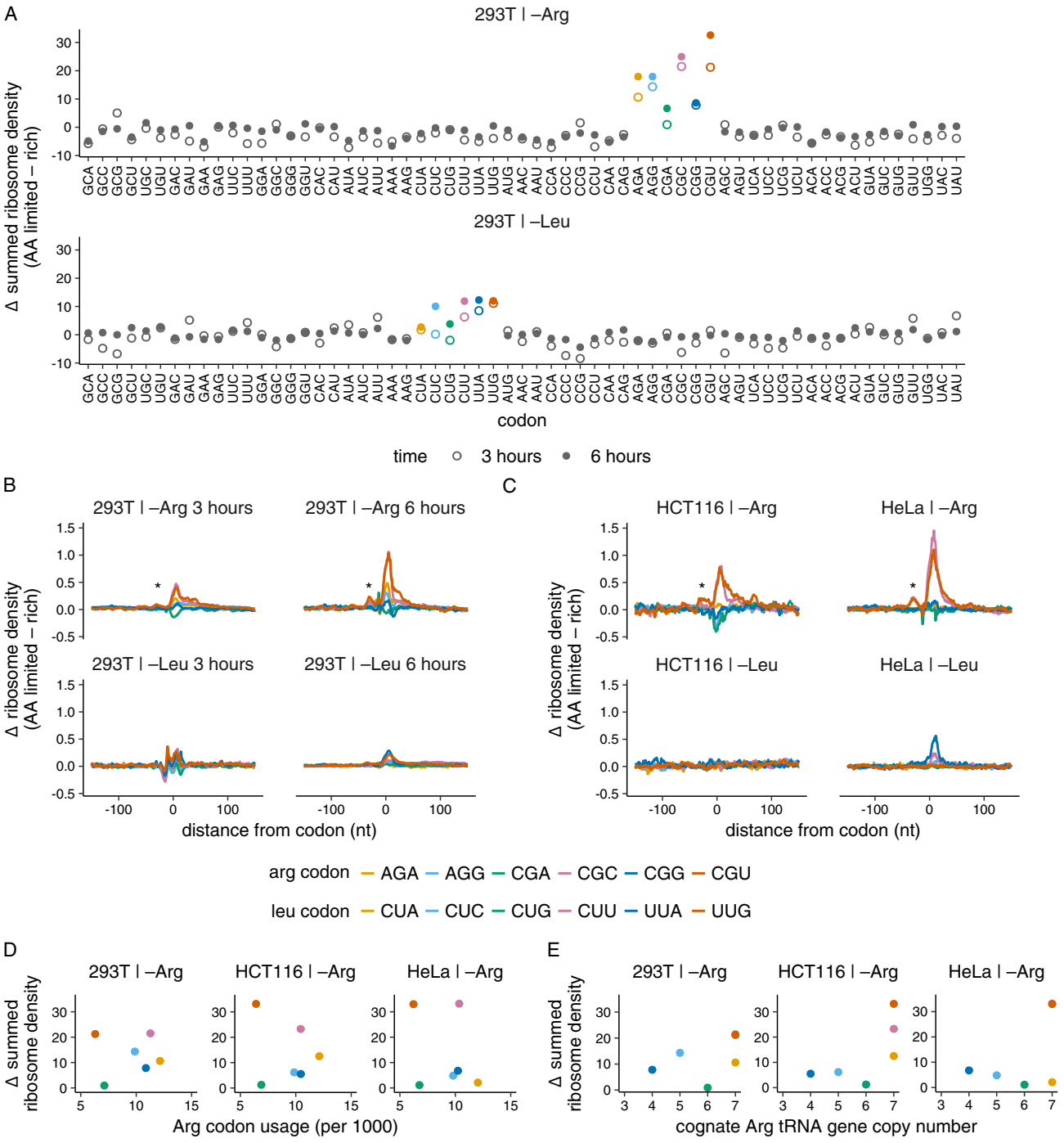

Figure 1. Codon-Specific Ribosome Pausing Emerges during Limitation for Arginine but Not Leucine

(A–C) Changes in codon-specific ribosome density in HEK293T cells, HCT116, and HeLa cells upon 3 or 6 hr of leucine (Leu) or arginine (Arg) limitation. Ribosome density for each codon is calculated relative to the mean footprint density for each coding sequence and averaged over all occurrences of the codon across detectably expressed transcripts (see STAR Methods for details). The difference in ribosome density between amino acid-limited and rich conditions across a 150 nt window around each codon is summed (A) or shown as such (B and C) (asterisks mark stalled trailing ribosomes). Arg and Leu codons are colored according to legend in (B) and (C).

(D and E) The summed change in ribosome density at Arg codons following 3 hr of Arg limitation in each cell line (see A and Figure S1H) is compared to the transcriptome usage frequency of Arg codons (see Figure S1J) (D) or genomic copy number of the cognate tRNA for each Arg codon (see Figure S1K) (E). Arg and Leu codons are colored according to legend in (B) and (C). Spearman rank correlation coefficient p-values all > 0.05.

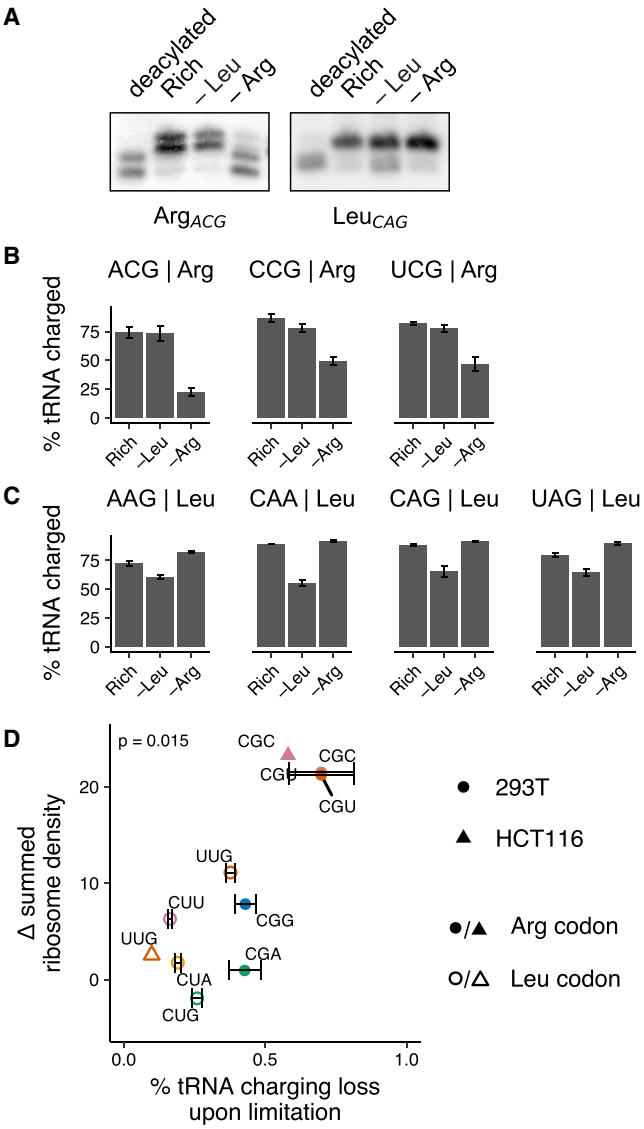

Figure 2. Selective Loss of tRNA Charging during Arginine Limitation

(A) Representative northern blots for determination of Arg and Leu tRNA charging levels in HEK293T cells following 3 hr of limitation for Leu or Arg or growth in rich medium. A control deacylated total RNA sample is used to identify uncharged tRNA species. tRNA probe is indicated below each blot (see STAR Methods for details; see Figure S2 for other blots).

(B and C) tRNA charging levels for 3 Arg (B) and 4 Leu tRNAs (C) in HEK293T cells following 3 hr of Leu or Arg limitation or growth in rich medium (calculated as described in STAR Methods). tRNA anticodon and isotype are indicated above plots; error bars represent the SEM from three technical replicates (see A and Figure S2 for representative blots and Figure S1L for codon-tRNA pairs).

(D) The summed change in ribosome density at Arg and Leu codons following 3 hr of Leu or Arg limitation in HEK293T and HCT116 cells (see Figure 1A) is plotted against the loss in charging for the cognate tRNA in the same condition. p indicates the p value of Spearman's rank coefficient, ρ (ρ = 0.7).

phosphorylated ribosomal protein S6 (P∼RPS6) reflected the same differential response (Figures S3A and S3B). GCN2 signaling was activated during limitation for both amino acids, as levels of the GCN2 target phosphorylated eIF2α (P∼eIF2α) increased to a similar extent (Figure 3B).

Our measurements of mTORC1 kinase activity mirrored downstream changes in ribosome density on mRNA targets of the pathway. 46 of 63 mRNAs that are translationally repressed by mTORC1 inhibition (Hsieh et al., 2012; Thoreen et al., 2012) had lower ribosome density during limitation for leucine than arginine (Figures 3C and 3E; Figures S3C, S3E, and S3G; Wilcoxon signed rank test p = 1.2e-5). mTORC1 signaling was also more repressed during limitation for leucine in HeLa cells (Figures 3C, 3E, and S3G; p = 0.0003). There was little mTORC1 or GCN2 signaling response to leucine limitation in HCT116 cells (Figures 3C–3F and S3G), consistent with our observation that leucine tRNA charging is largely unaffected (Figure S2C).

Comparing downstream changes in ribosome density on mRNA targets of ATF4 and CHOP, transcriptional effectors downstream of GCN2 (Han et al., 2013), during arginine versus leucine limitation revealed subtle but consistent differential GCN2 responses. In HEK293T cells, the ATF4/CHOP target response was similar during limitation for leucine and arginine (Figures 3D, 3F, S3D, S3F, and S3G; Wilcoxon signed rank test p = 0.33). However, GCN2 became significantly more activated during arginine limitation after a longer duration of amino acid limitation (Figures S3D and S3F; p = 5.7e-4), which also increased ribosome pausing (Figures 1A and 1B). GCN2 was also more activated during limitation for arginine in the HCT116 and HeLa cell lines (Figures 3D, 3F, and S3G; p = 9.3e-7 and 1.8e-12, respectively). The GCN2 response was most robust in the conditions and cell lines in which ribosome pausing was most severe, consistent with the recent observation that GCN2 may be activated downstream of ribosome pausing (Ishimura et al., 2016).

The variability of the signaling responses across all three cell lines was surprising, given that we observed a conserved signature of ribosome pausing. However, if pausing is determined by the extent to which the amino acid supply and demand are matched under each condition, then it may be the totality of the signaling response, rather than the activity of each single pathway, that regulates this balance. We sought to test this idea in the HEK293T cell line, in which ribosome pausing emerges only during arginine limitation, in the context of a relatively weaker overall signaling response compared to leucine limitation.

An Insufficient mTORC1 and GCN2 Response to Amino Acid Limitation Induces Ribosome Pausing

The mTORC1 and GCN2 pathways inhibit the initiation phase of protein synthesis in response to amino acid limitation (Sonenberg and Hinnebusch, 2009). This lowers the number of elongating ribosomes, which are major consumers of the cytosolic amino acid pool. If this combined signaling response does not sufficiently reduce arginine consumption during its limitation, tRNA charging loss and ribosome pausing could result. Specifically, if residual mTORC1 activity and/or inadequate activation of GCN2 drives loss of tRNA charging and ribosome pausing, we hypothesized that increasing the response of these pathways would reduce pausing upon arginine limitation, and conversely, that decreasing their response would induce pausing upon leucine limitation.

We first inhibited mTOR kinase activity with Torin1 (Thoreen et al., 2009) during both arginine and leucine limitation (Figure 4A) and found that charging of all arginine and leucine tRNAs tested increased back to baseline rich condition levels (Figure S4A). Torin1 treatment also prevented an increase in ribosome density at any codon upon leucine or arginine limitation (Figures 4B and S4B), demonstrating that mTORC1 inhibition during amino acid limitation is sufficient to block depletion of the cognate charged tRNA fraction and ribosome pausing.

Next, we tested whether loss of the mTORC1 response to amino acid limitation would exacerbate tRNA charging loss and ribosome pausing. We rendered mTORC1 insensitive to amino acid levels by overexpression of a constitutively active form of its upstream regulator, the GTPase Ras related GTP binding B (RRAGB, cell line RagB-Q99L) (Sancak et al., 2008) (Figure 4C). The RagB-Q99L cell line exhibited reduced leucine tRNA charging during leucine limitation; charging fell to 22% for $tRNA^{Leu}_{CAA}$, which decodes the codon UUG (Figure S4C). Compared to a control line that overexpressed humanized *R. reniformis* GFP (hrGFP), constitutive mTORC1 activity increased charging loss due to leucine limitation by 50%. Charging was also reduced by 36% due to constitutive mTORC1 activity upon leucine limitation for $tRNA^{Leu}_{AAG}$, which decodes CUU (Figure S4C). Concordantly, minor ribosome pausing emerged at the leucine codons UUG and CUU (Figure S4D). Little difference was detected in arginine tRNA charging or ribosome pausing at arginine codons upon arginine limitation (Figures S4C and S4D), and we thus repeated these measurements after 6 hr, rather than 3 hr, of amino acid limitation to reveal their dynamics over time.

After prolonged amino acid limitation, the RagB-Q99L cell line exhibited further increased tRNA charging loss and ribosome pausing compared to control cell lines. Charging fell as low as 18% for $tRNA^{Leu}_{CAA}$ (Figure S4E), and ribosome pausing emerged at the cognate leucine codon UUG as well as the CUC and CUU codons (Figures 4F and S4F). Similarly, the proportion of charged $tRNA^{Arg}_{ACG}$ fell to 19% (Figure S4E), and ribosome pausing increased at the cognate arginine codons CGC and CGU (Figures 4F and S4F). Ribosome pausing was also increased slightly in the hrGFP control cell line relative to unmodified HEK293T cells (wild-type [WT]) (Figures 4F and S4F), possibly due to the translational burden of transgene overexpression (Elf et al., 2003). In summary, constitutive mTORC1 activation significantly worsened tRNA charging loss and exacerbated ribosome pausing during both leucine and arginine limitation.

We next investigated the role of GCN2 in ribosome pausing. We generated a GCN2 knockout (KO) cell line (Figure S4G) in which eIF2α was not phosphorylated in response to amino acid limitation (Figure 4D). GCN2 activation is reported to be necessary for inhibition of mTORC1 signaling upon leucine or arginine limitation (Averous et al., 2016); we confirmed that there is no significant mTORC1 response to those conditions in our GCN2 KO cell line (Figure 4E).

tRNA charging loss and ribosome pausing were greatly amplified in the GCN2 KO cell line. $tRNA^{Leu}_{CAA}$ charging fell to 14% upon leucine limitation (Figure S4E), and ribosome density at the cognate UUG leucine codon rose substantially, with an average of four ribosomes stalled behind the paused ribosome (Figures 4F and S4F). Pausing increased only slightly at the arginine CGC and CGU codons (Figures 4F and S4F), although $tRNA^{Arg}_{ACG}$ charging continued to drop (Figure S4E), indicating that pause duration is approaching an upper limit at these codons. Indeed, significant ribosome pausing emerged at the AGA arginine codon (Figures 4F and S4F), suggesting that charging of a second arginine isoacceptor, $tRNA^{Arg}_{UCU}$, is exhausted upon arginine limitation in the GCN2 KO cell line. Together, these results indicate that the absence of a response through the GCN2 or mTORC1 pathways during amino acid limitation is sufficient to deplete charged tRNA pools and induce extensive genome-wide ribosome pausing at cognate codons, consistent with our hypothesis that an insufficient signaling response can drive consumption of the limiting amino acid into a substrate-limited regime for protein synthesis.

In addition to their control over translation, mTORC1 and GCN2 regulate other critical functions, such as metabolism and autophagy (Sonenberg and Hinnebusch, 2009), which could affect intracellular amino acid levels. To test our hypothesis that levels of an amino acid during its limitation are primarily set by the demand from translation elongation, we briefly exposed cells limited for leucine or arginine to the elongation inhibitor cycloheximide. This significantly restored $tRNA^{Leu}_{CAA}$ and $tRNA^{Arg}_{ACG}$ charging (Figure S4H), indicating that the flux of arginine and leucine into translation is a key determinant of the cytosolic levels of these amino acids upon their limitation. Thus, ribosome pausing during limitation for an amino acid is likely determined by the degree of translational control imposed by mTORC1 and GCN2.

Genome-wide Ribosome Pausing Reduces the Global Protein Synthesis Rate during Arginine Limitation

Having examined the upstream determinants of ribosome pausing, we next sought to investigate its impact on cellular translation. We measured the global protein synthesis rate during limitation of leucine or arginine by quantifying incorporation of the antibiotic puromycin into nascent polypeptides (Schmidt et al., 2009). In line with previous measurements (Scott et al., 2000), we found that global protein synthesis rate was consistently lower during limitation for arginine than leucine (Figures 5A, 5B, and S5A).

We considered three processes that could contribute to the regulation of translation during amino acid limitation: mTORC1 inhibition, GCN2 activation, or ribosome pausing. Given that mTORC1 activity, which stimulates translation initiation, is higher during arginine than leucine limitation in HEK293T cells (Figures 3A, 3C, and 3E), the mTORC1 response cannot account for lower global protein synthesis during arginine limitation. The principal difference between GCN2- and pausing-mediated control over translation is that GCN2 regulates initiation, while ribosome pausing regulates elongation. To assess which mechanism accounts for the greater reduction of global protein synthesis rate upon arginine versus leucine limitation, we used polysome profiling to determine the average number of ribosomes per transcript in each condition. If the global protein synthesis rate is lower during arginine limitation due to inhibition of initiation, then there would be fewer ribosomes per transcript upon

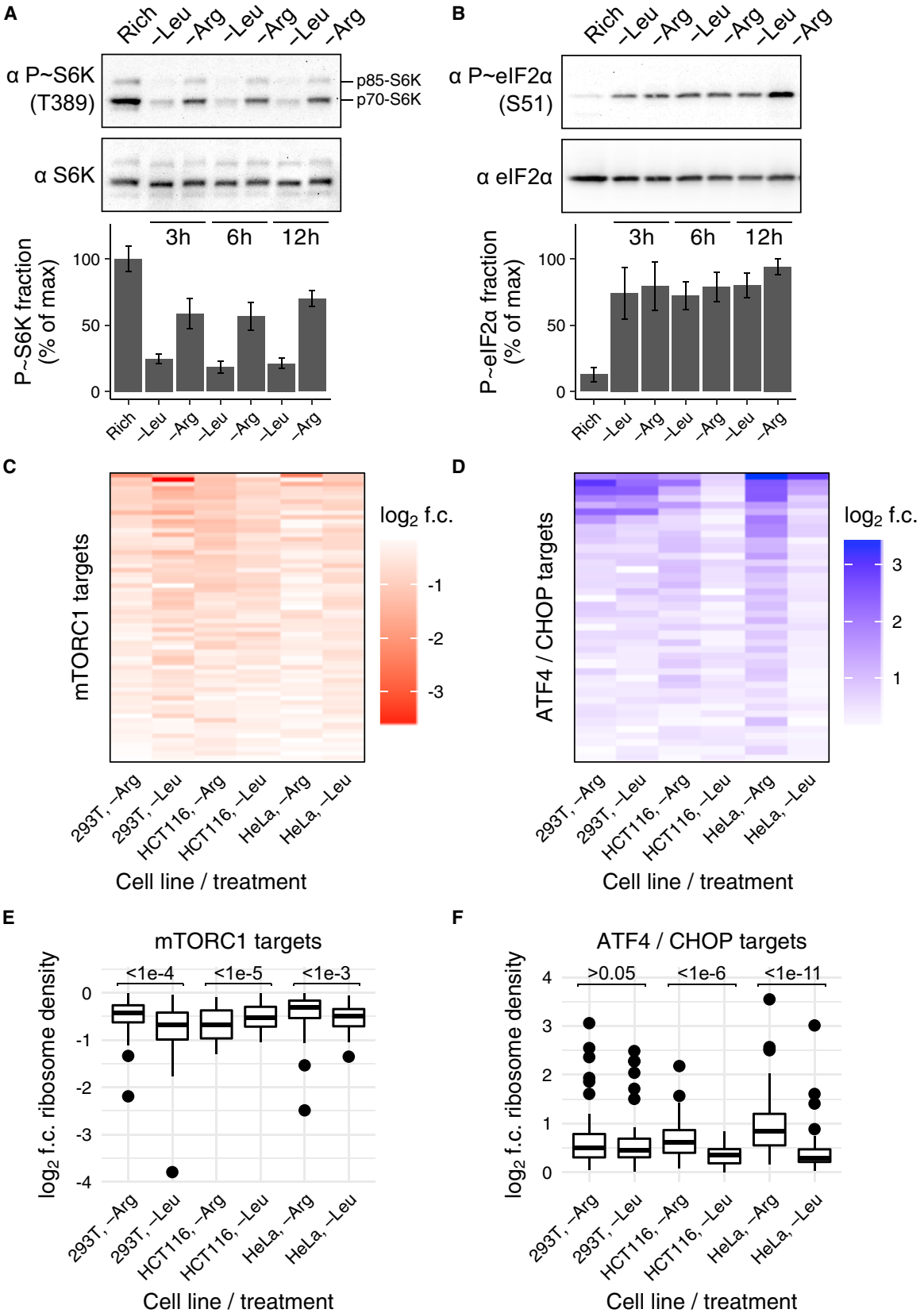

(legend on next page)

limitation for arginine compared to leucine. Instead, if the global protein synthesis rate is reduced by slow elongation, then we would find relatively more ribosomes per transcript upon arginine limitation. While the polysome fraction was reduced by limitation for leucine or arginine, it was consistently higher during arginine than leucine limitation (Figures 5C and S5B), indicating that there are more ribosomes per transcript during arginine limitation despite a lower global protein synthesis rate. Thus, elongation rate control must account for the greater repression of global protein synthesis rate upon arginine limitation.

Elongation rate could be reduced by a global mechanism or by ribosome pausing during arginine limitation. For example, global elongation rate control can be executed by reduced eukaryotic elongation factor 2 (EEF2) activity due to phosphorylation by EEF2 kinase (EEF2K) downstream of mTORC1 inhibition (Leprivier et al., 2013). To assess the role of EEF2K, we generated an EEF2K KO cell line (Figures S5C and S5D). Loss of general elongation factor regulation by EEF2K increased the global protein synthesis rate upon arginine and leucine limitation by a similar, small margin (Figure S5E). Therefore, downregulation of global elongation factor activity cannot explain the greater reduction of protein synthesis upon arginine than leucine limitation, and we instead attribute this difference to ribosome pausing.

To isolate the contribution of ribosome pausing to global protein synthesis rate reduction, we made use of the GCN2 KO cell line, which lacks an initiation rate control response to amino acid limitation through both the GCN2 and mTORC1 pathways (Harding et al., 2000) (Figures 4D and 4E). We reasoned that any residual inhibition of the global protein synthesis rate during leucine or arginine limitation in the GCN2 KO cell line would be due to ribosome pausing. The global protein synthesis rate was reduced by 25% during arginine limitation (Figures 5D and S5F). Strikingly, despite this lower global protein synthesis rate, there was a higher polysome fraction during arginine limitation than in rich conditions in this cell line (Figures 5E and S5B), consistent with our observation of strong ribosome pausing under these conditions (Figure 4F). Ribosomes also pause at a leucine codon in the GCN2 KO cell line, and accordingly, the polysome fraction was higher upon leucine limitation than in rich conditions as well (Figure 5E). However, there was no change in the global protein synthesis rate upon leucine limitation in the GCN2 KO cell line (Figures 5D and S5F), suggesting that the global protein synthesis rate in this condition in WT cells is primarily reduced by the mTORC1 and/or GCN2 responses. In sum, the inverse relationship between global protein synthesis rate and ribosome loading per transcript upon arginine limitation supports a model in which ribosome pausing reduces the global protein synthesis rate.

Pause-Site Codons in mRNAs Reduce Protein Expression and Induce Premature Termination of Translation

We next investigated whether pausing on mRNAs specifically inhibits production of the encoded protein. Toward this goal, we adapted a protein synthesis reporter in which YFP is fused to an engineered unstable *E. coli* dihydrofolate reductase (DHFR) domain (Han et al., 2014). In this reporter system, the unstable reporter is rapidly degraded and fluorescence only accumulates upon addition of a stabilizing ligand, trimethoprim (TMP) (Figure S6A). Fluorescence upon arginine and leucine limitation correlated with the global protein synthesis rates that we measured in those conditions (Figure S6A versus Figures 5A and 5B), suggesting that it faithfully reflects the protein synthesis rate of the reporter. To determine the specific effect of ribosome pausing on the reporter protein synthesis rate, we constructed a set of codon variant reporters in which either all arginine codons or all leucine codons were swapped to each of the six arginine or leucine codons, respectively (Figure 6A).

We first determined whether the pause-site arginine codons, CGC and CGU, would reduce reporter protein synthesis rate during arginine limitation. In all three cell lines in which we detected ribosome pausing upon arginine limitation (Figures 1A–1C), the YFP-DHFR synthesis rate was reduced during arginine limitation when the pause-site codons CGC or CGU were used to encode arginine (YFP-CGC or YFP-CGU) (Figure 6B, left plot; Figures S6B and S6C). The YFP-AGA synthesis rate was also reduced in HEK293T cells (Figure 6B, left plot; Figure S6B), suggesting that pausing may emerge at this codon after an extended duration of arginine limitation. In the GCN2 KO cell line, in which ribosomes pause at CGC, CGU, and AGA codons (Figure 4F), the use of each of these codons also reduced YFP synthesis rate upon arginine limitation (Figure 6C). Importantly, there was little difference in the measured protein synthesis rates between the arginine codon variants upon leucine limitation (Figures 6B, 6C, S6B, and S6C). Similarly, the six leucine codon variants had comparable reductions in YFP synthesis rate upon leucine or arginine limitation (Figures 6D and S6B), consistent with the absence of ribosome pausing at these codons in WT cells (Figure 1A–1C). However, the YFP-UUG synthesis rate was strongly reduced in the GCN2 KO cell line upon limitation for leucine, reflecting the emergence of ribosome pausing at

Figure 3. Differential mTORC1 and GCN2 Responses to Arginine and Leucine Limitation

(A and B) Representative western blots for phosphorylated and total levels of ribosomal protein S6 kinase 1 (S6K) (A) or eIF2α (B) in HEK293T cells after growth in rich medium or after 3, 6, or 12 hr of Leu or Arg limitation. Bar graph shows percent of protein that is phosphorylated in each condition relative to the maximum. Error bars represent the SEM from three technical replicates.

(C and D) Heatmap of $\log_2$ fold-change (f.c.) in ribosome density for mRNA targets of mTORC1 inhibition (Hsieh et al., 2012) (C) or GCN2 activation via ATF4/CHOP (Han et al., 2013) (D) following 3 hr of Leu or Arg limitation relative to growth in rich medium for HEK293T, HCT116, and HeLa cells. Only targets with a $\log_2$ fold change of <0 (for mTORC1 targets) or >0 (for ATF4/CHOP targets) were considered. In HEK293T, HCT116, and HeLa cells, 46 out of 63 (73%), 14 out of 63 (22%), and 45 out of 63 (71%) mTORC1 targets (C) and 26 out of 40 (65%), 35 out of 40 (88%), and 40 out of 40 GCN2 targets (D) had higher ribosome density upon Arg than Leu limitation, respectively.

(E and F) Boxplot of the $\log_2$ fold change for each mTORC1 (E) or ATF4/CHOP (F) target upon amino acid limitation. A two-sided Wilcoxon signed rank test was performed with $\mu = 0$; the resulting p value is shown for each comparison (see STAR Methods for details). In HEK293T, HCT116, and HeLa cells, mTORC1 activity (E) was 1.2-, 0.9-, and 1.1-fold higher and GCN2 activity (F) was 1-, 1.2-, and 1.5-fold higher during limitation for Arg, respectively.

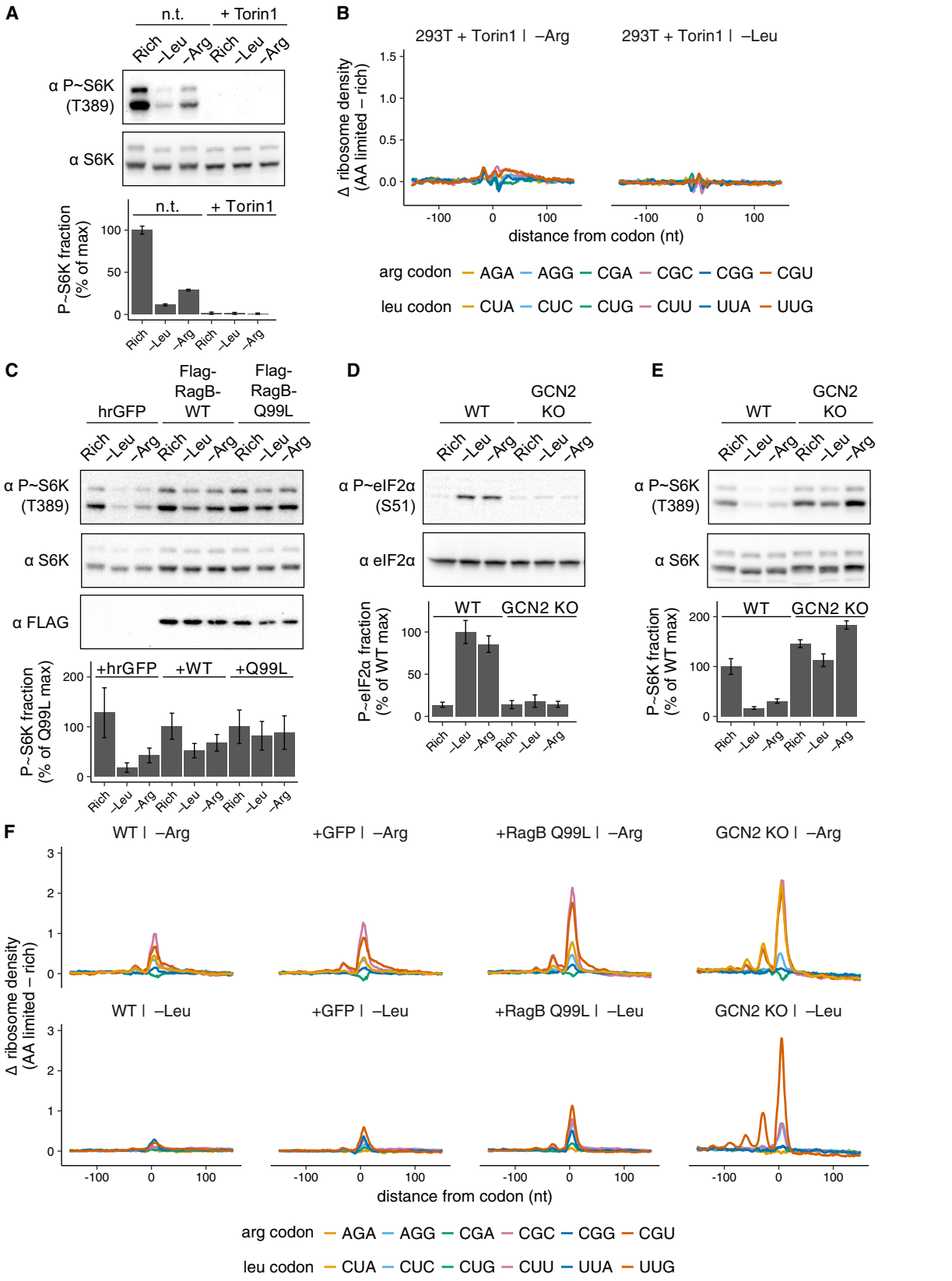

(legend on next page)

this codon in this condition (Figures 6E and 4F). In all cases, ribosome pausing upon amino acid limitation was sufficient to inhibit reporter protein synthesis.

Recent work suggests a role for mRNA degradation in reduced protein production due to slow translation of rare codons in yeast (Presnyak et al., 2015; Radhakrishnan et al., 2016). To determine whether lower YFP production rates could be explained by reporter mRNA degradation downstream of ribosome pausing, we measured changes to YFP-CGC and YFP-CGG reporter mRNA levels during arginine and leucine limitation. Levels of YFP-CGC, which contains pause sites, were 2-fold higher than levels of YFP-CGG, which does not contain pause sites, in each condition (Figure S6D). YFP-CGC and YFP-CGG levels were similarly reduced by 50% upon arginine limitation and unaffected by leucine limitation (Figure S6D). Thus, pausing is not clearly linked to a reduction in mRNA levels, and such an effect cannot explain why less protein is produced from the YFP-CGC reporter specifically upon arginine limitation.

To determine whether premature abortive termination of translation might instead account for the reduction in the protein synthesis rate by ribosome pausing, as previously described in bacteria (Subramaniam et al., 2014), we inserted a tandem repeat of eight pause-site (UUG) or non-pause-site (CUA) leucine codons in between the YFP and DHFR domains (Figures 6F). Full-length YFP-DHFR is degraded efficiently, resulting in little fluorescence (Figure S6A). However, abortive termination at the pause-site codons would prevent synthesis of the DHFR degron and generate stable YFP. Indeed, we observed a 100-fold increase in the YFP fluorescence specifically upon leucine limitation when 8 pause-site UUG leucine codons were inserted (UUG8), and this reporter was expressed in the GCN2 KO cell line (Figure 6G). The size of the stable UUG8 reporter protein corresponded to the predicted size of the premature truncation product (Figure 6I). By contrast, we detected only a minor fluorescence increase in the CUA8 reporter upon leucine limitation (Figure 6G), and the size of the polypeptide produced corresponded to the full-length reporter (Figures 6I and S6F). There was no evidence for premature termination of UUG reporter translation in any cell line or condition in which there is no pausing at UUG codons (Figures 6G and 6H). Premature termination correlated positively with the number of pause-site codons in the reporter, was detectable when as few as two pause sites were present (Figure 6H), and did not reduce mRNA levels (Figure S6E). It was in fact associated with increased reporter mRNA levels, which may be explained by increased ribosome loading due to stalling upstream of tandem pause sites. We did not find evidence for similar levels of premature termination at arginine codons during arginine limitation in WT cells, perhaps because premature termination products with polyarginine tracts are degraded (Brandman and Hegde, 2016).

Based on our observation that ribosome pausing reduces protein expression, we sought to identify endogenous proteins that might be regulated by pause-site codons during arginine limitation. We calculated the bias in usage of the pause-site arginine codons CGC and CGU for 18,660 endogenous coding sequences based on the genome-wide average usage frequency of these codons (Figure S6G). Coding sequences biased against use of pause-site arginine codons were significantly enriched for gene ontology (GO) terms related to organelle organization, macromolecule and nitrogen-compound metabolism, RNA processing, and positive regulation of GTPase activity (Figure S6H). Conversely, genes with bias in favor of CGC and CGU codons were significantly enriched for GO terms related to nucleosomes, intermediate filaments, and ion channels (Figure S6H). Given our evidence that ribosome pausing can regulate protein production and stimulate premature termination, genes enriched in pause sites are likely to be more translationally repressed upon a shift to arginine-limited conditions than those depleted of pause sites.

DISCUSSION

Our study provides a mechanistic dissection of the cause and consequences of ribosome pausing due to amino acid limitation in mammalian cells. We reveal an evolutionarily conserved role for synonymous codon-specific ribosome pausing in the regulation of protein synthesis during amino acid limitation, a phenomenon that has been previously observed only in bacteria (Subramaniam et al., 2013b, 2014). We found a layer of complexity in this process that is unique to mammalian cells: quantitative differences in the signaling response to limitation for two amino acids results in qualitative differences in ribosome pausing.

Despite recent evidence that tRNA levels or synonymous codon usage can influence translation in mammalian systems (Gingold et al., 2014; Goodarzi et al., 2016; Saikia et al., 2016), we did not find a correlation between ribosome pausing and these quantities upon arginine limitation. Notably, the codons at which ribosomes pause during amino acid limitation in bacteria are also not necessarily rare codons or decoded by low abundance tRNAs (Subramaniam et al., 2013a, 2013b, 2014). It is likely that the balance between tRNA supply and codon usage demand determines differential isoacceptor tRNA sensitivity to

Figure 4. Signaling through the mTORC1 and GCN2 Pathways Regulates the Magnitude of Ribosome Pausing during Amino Acid Limitation

(A) Representative western blots for phosphorylated and total S6K in HEK293T cells after growth in rich medium or limitation for Leu or Arg for 3 hr, with (+ Torin1) or without (n.t.) 250 nM Torin1. Bar graph shows the percentage of protein that is phosphorylated relative to the maximum.

(B) Changes in codon-specific ribosome density in the hrGFP cell line (see C) after 3 hr of Leu or Arg limitation with 250 nM Torin1 relative to rich medium.

(C) Representative western blots for phosphorylated S6K, total S6K, and FLAG after growth in rich medium or 3 hr of Leu or Arg limitation in HEK293T cells expressing hrGFP, FLAG-RagB-WT (RagB-WT), or FLAG-RagB-Q99L (RagB-Q99L). Bar graph shows the percentage of protein that is phosphorylated relative to the maximum in the RagB-Q99L cell line.

(D and E) Representative western blots for phosphorylated and total eIF2α (D) or S6K (E) after growth in rich medium or 3 hr of Leu or Arg limitation in the HEK293T (WT) or GCN2 KO cell lines. Bar graphs show the percentage of protein that is phosphorylated relative to the maximum in WT cells.

(F) Changes in codon-specific ribosome density for WT, hrGFP, FLAG-RagB-Q99L, and GCN2 KO cell lines following 6 hr of limitation for Leu or Arg relative to rich medium.

In (A) and (C)–(E), error bars represent the SEM from three technical replicates.

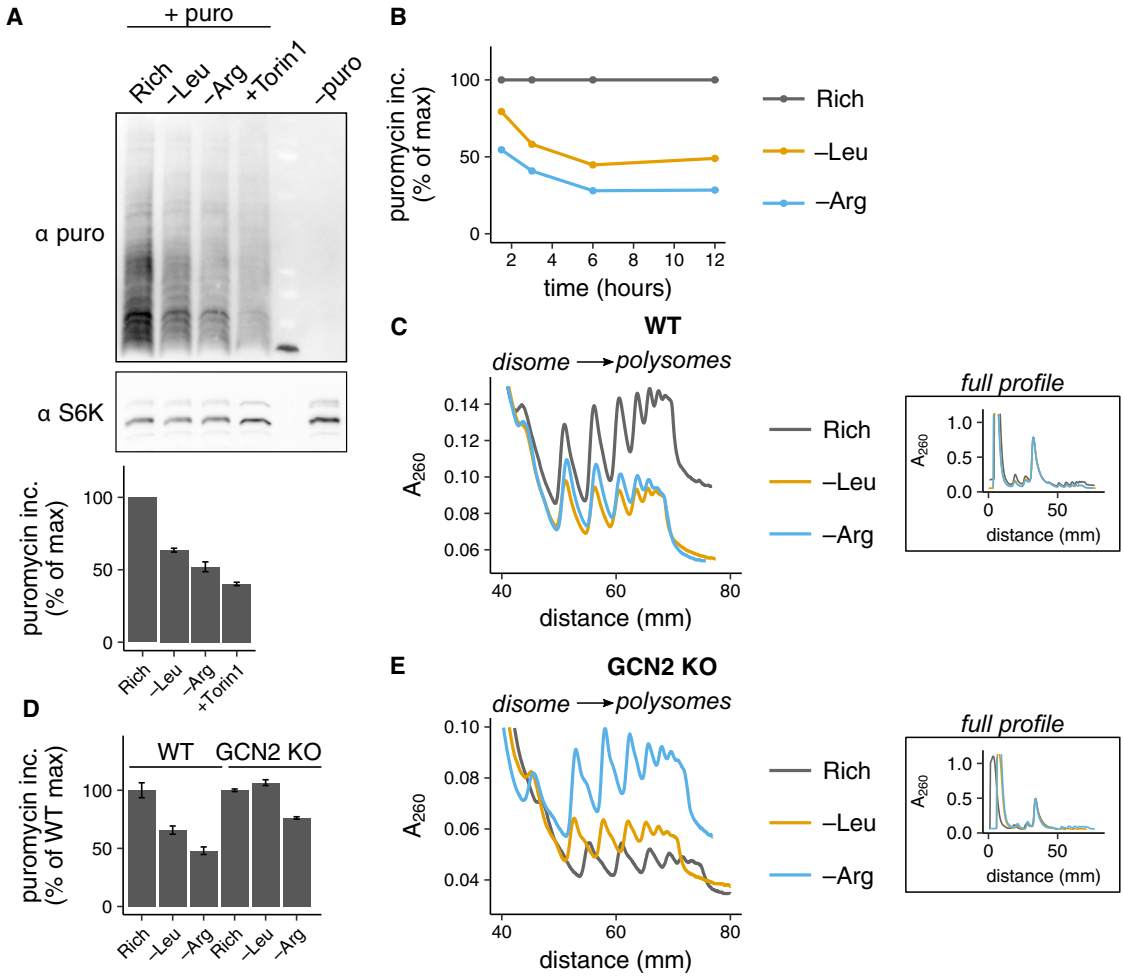

Figure 5. Ribosome Pausing Reduces Global Protein Synthesis Rate during Amino Acid Limitation

(A) Representative western blots for puromycin and S6K in HEK293T cells after (+ puro) or without (– puro) a pulse of 10 μg/mL puromycin following 3 hr of Leu or Arg limitation, treatment with 250 nM Torin1, or growth in rich medium. Bar graph shows puromycin incorporation relative to rich medium (calculated as described in STAR Methods).

(B) Puromycin incorporation in HEK293T cells following 1.5, 3, 6, or 12 hr of Leu or Arg limitation relative to rich medium.

(C) Polysome profiles from HEK293T (WT) cells following 6 hr of Leu or Arg limitation or growth in rich medium. The main plot shows overlaid polysome profiles starting at the disome (2 ribosome) peak and the inset plots show the entire profile, aligned with respect to the monosome peak height along the y axis and position along the x axis.

(D) Puromycin incorporation in WT or GCN2 KO cell lines following 3 hr of Leu or Arg limitation relative to rich medium (calculated as in described in STAR Methods; see Figure S5G for representative blots).

(E) Polysome profiles (as described in C) from the GCN2 KO cell line following 6 hr of limitation for leucine or Arg or growth in rich medium.

In (A) and (D), error bars represent the SEM from three technical replicates.

changes in arginine levels, as observed in bacteria (Dittmar et al., 2005; Elf et al., 2003). We propose that consideration of both nutrient context and sensitivity to nutrient fluctuations is critical for defining which codons or tRNAs are functionally optimal with respect to translation efficiency. Additionally, our measurements of tRNA charging loss upstream of ribosome pausing upon amino acid limitation suggest that even a 50% charging level for many tRNAs was insufficient to cause ribosome pausing at the cognate codons. This reflects a robustness of ribosome elongation rate to fluctuations in charged tRNA concentrations and is consistent with the proposal that tRNA abundance in mammals is unlikely to be evolutionarily optimized for globally efficient translation (Galtier et al., 2018).

Our finding that the mTORC1 and GCN2 pathways respond more potently to limitation for different single amino acids highlights an unusual divergence in their roles, challenging the idea that the pathways act coordinately to sense amino acid limitation and appropriately regulate translation (Park et al., 2017). The mTORC1 response is clearly nonoptimal with respect to preserving arginine homeostasis for protein synthesis; it responds

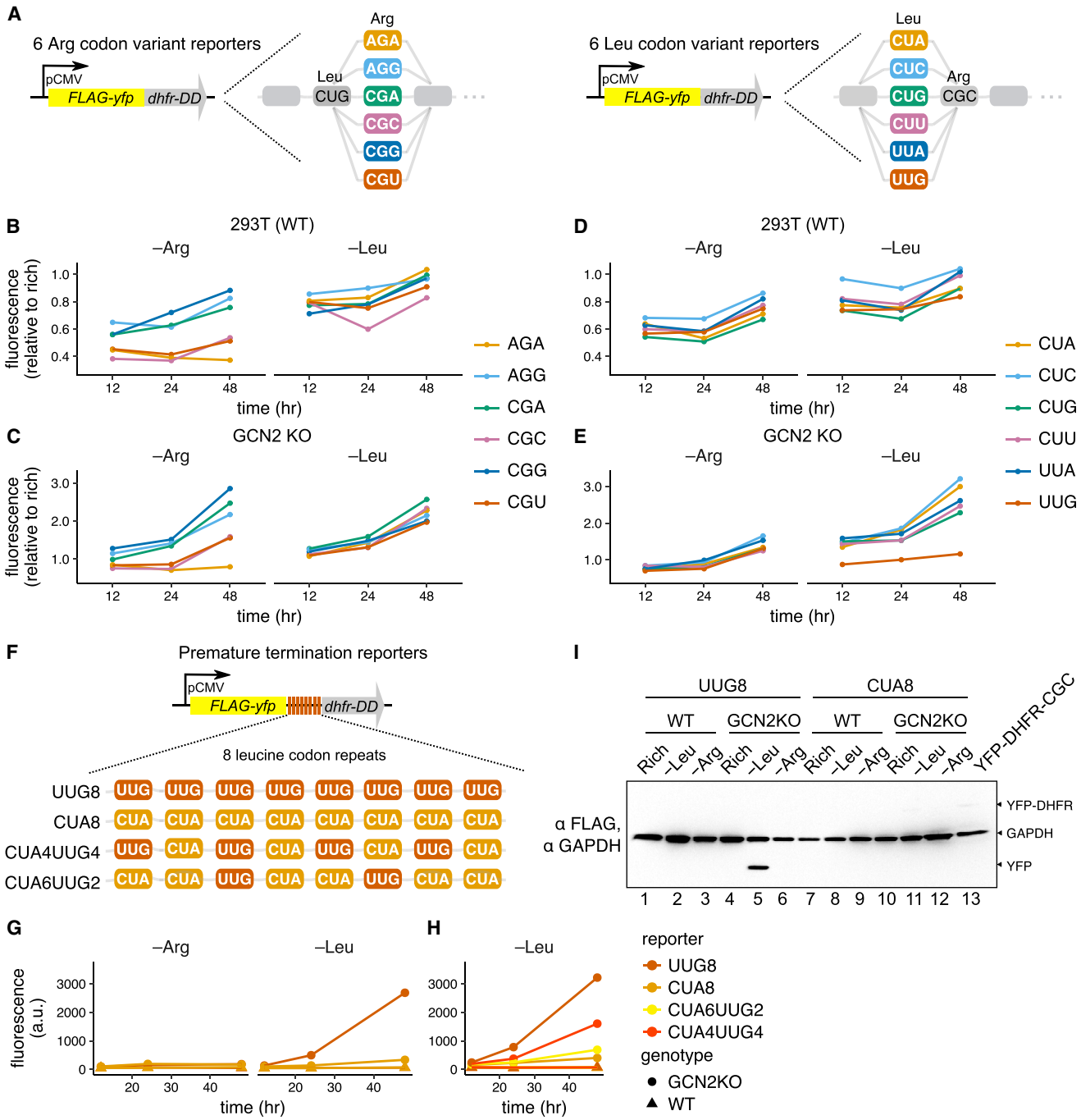

Figure 6. Ribosome Pausing Reduces Protein Expression from Reporter mRNAs and Induces Premature Termination of Translation

(A) Arg and Leu YFP codon variant reporter design (see STAR Methods for details).

(B–E) YFP fluorescence in the HEK293T (WT) (B and D) or GCN2 KO cell lines (C and E) stably expressing the Arg (B and C) or Leu (D and E) YFP codon variant reporters following limitation for Leu or Arg with 10 μM trimethoprim (+TMP) for 12, 24, or 48 hr relative to rich medium +TMP.

(F) Premature termination reporter design. A short linker of 8 tandem CUA or UUG leucine codons was added to the YFP-CUA reporter (as shown in A).

(G and H) YFP fluorescence in the WT or GCN2 KO cell lines expressing the UUG8, CUA8 (G and H) CUA6UUG2, or CUA4UUG4 (H) reporters following limitation for Leu or Arg for 12, 24, or 48 hr without TMP.

(I) Western blot for FLAG epitope and GAPDH in the WT or GCN2 KO cell lines expressing the UUG8 or CUA8 reporters after growth in rich medium or 48 hr of Leu or Arg limitation. Lane 13 contains lysate from the YFP-WT reporter cell line for a full-length reporter size reference; GAPDH provides an intermediate size reference (see Figure S6F for overexpressed blot).

more weakly to arginine than leucine limitation, even though arginine becomes more rate limiting for translation than leucine. Given that direct sensors for arginine (Chantranupong et al., 2016; Wang et al., 2015) and leucine (Wolfson et al., 2016) have been identified in the mTORC1 pathway, this observation is surprising. One possibility is that in the context of a tissue or an organism, arginine limitation might be typically accompanied by additional cues to stimulate an optimal mTORC1 response, and limitation for only arginine *in vitro* is insufficient to evoke this response. Investigating the response to arginine limitation *in vivo* will shed light on the role of mTORC1 in regulating arginine consumption.

In contrast to mTORC1, GCN2, which senses uncharged tRNA, appears to respond optimally; it is equally or more strongly activated during arginine than leucine limitation. This raises the question of why a robust GCN2 response is insufficient to prevent pausing. It was recently shown that GCN2 can directly sense ribosome pausing (Ishimura et al., 2016). GCN2 activation may in part be downstream of the emergence of ribosome pausing, thus responding to, rather than preventing, the loss of amino acid homeostasis in translation.

Although we find that the signaling response to amino acid limitation is necessary to prevent ribosome pausing in HEK293T cells, we note that other mechanisms may exert control over pausing in distinct cell types. For example, rates of protein catabolism, proliferation, or lysosomal amino acid content could alter the intracellular amino acid supply and demand balance. Indeed, we find no ribosome pausing upon limitation for leucine in HCT116 cells despite a weak amino acid signaling response (Figures 3C–3F, S3G, and 1C). An investigation in multiple cell types will clarify the range of mechanisms that control ribosome pausing.

We find that ribosome pausing reduces both global and gene-specific protein synthesis rates. The effects of slow translation at specific codons on protein production have been widely linked to mRNA decay; recent work in yeast has suggested that ribosome stalling at nonoptimal codons represses protein synthesis rates by increasing mRNA decay rates (Presnyak et al., 2015; Radhakrishnan et al., 2016; Simms et al., 2017). We did not find evidence for a reduction in mRNA levels due to pausing, though we cannot exclude an increase in the mRNA decay rate balanced by an increased synthesis rate. Significant changes in mRNA levels have not been observed in cases where protein production is altered by ribosome pausing at specific codons during amino acid limitation (Saikia et al., 2016; Subramaniam et al., 2013b, 2013a, 2014). Perhaps pausing due to loss of tRNA charging is qualitatively different from "no-go" pauses that result from overall tRNA scarcity and thus might not stimulate no-go decay (Buskirk and Green, 2017). We did find evidence for truncated nascent peptides upon ribosome pausing at leucine codons, suggesting that pausing due to limiting charged tRNA can trigger abortive termination of translation, although the factors involved remain to be elucidated.

Dysregulated amino acid signaling and elevated proliferative demand for amino acids are characteristic features of many cancers (Saxton and Sabatini, 2017; Vander Heiden and DeBerardinis, 2017). Ribosome pausing may thus occur across a range of malignant states *in vivo*, raising the question of whether this response is deleterious, neutral, or adaptive. In bacteria, ribosome stalling during amino acid limitation can act as a sensor for upregulating amino acid biosynthesis genes and entry into a biofilm state, suggesting an adaptive role (Subramaniam et al., 2013b, 2013a). Our finding that genes involved in nucleotide metabolism are biased against the use of arginine pause site codons is intriguing, as arginine is a substrate for nucleotide synthesis, that can be limiting for cancer cell proliferation (Rabinovich et al., 2015). Histone genes are biased toward the use of pause sites, and reduced nucleosome synthesis could in part underlie the S-phase cell-cycle arrest that accompanies arginine limitation (Scott et al., 2000), though it is unclear whether this would be adaptive. We find that ribosome pausing correlates with reduced cell viability (Figure S6I), consistent with reports that arginine limitation induces death in certain cancer cell lines (Scott et al., 2000). Therefore, pausing may have a deleterious effect on the cell, for example via protein misfolding or mistranslation stress (Drummond and Wilke, 2008). To assess whether ribosome pausing is a targetable metabolic vulnerability, it will be important to determine in these and other contexts whether it adapts cellular metabolism and gene expression to amino acid limitation or increases cellular stress.

STAR★METHODS

Detailed methods are provided in the online version of this paper and include the following:

- KEY RESOURCES TABLE
- CONTACT FOR REAGENT AND RESOURCE SHARING
- EXPERIMENTAL MODEL AND SUBJECT DETAILS
  - Human cell line culture
  - Limitation for single amino acids
- METHOD DETAILS
  - Construction of plasmids
  - Stable cell line generation
  - Ribosome profiling
  - Polysome profiling
  - Intracellular amino acid quantitation
  - tRNA charging analysis
  - Western and dot-blotting
  - Northern blotting
  - Flow cytometry
  - Puromycin incorporation assays
  - Reverse transcription & qPCR
  - Cell viability assays
- QUANTIFICATION AND STATISTICAL ANALYSIS
  - Databases utilized
  - Ribosome profiling data analysis
  - Estimation of usage bias for pause-site arginine codons and GO analysis
  - Statistics
- DATA AND SOFTWARE AVAILABILITY

SUPPLEMENTAL INFORMATION

Supplemental Information includes six figures and can be found with this article online at https://doi.org/10.1016/j.molcel.2018.06.041.

ACKNOWLEDGMENTS

We thank B. Zid, C. Chidley, T. Pan, A. Murray, V. Denic, V. Mootha, and the O'Shea lab for helpful discussions; J. Piechura and J. Darnell for comments on the manuscript; and C. Shoemaker and K. Han for reagents and advice. We thank C. Daly, K. Chatman, and the Flow Cytometry Core at the Harvard Bauer Core Facilities. Sequencing data analysis was run on the Odyssey cluster (supported by Harvard Research Computing) and the Rhino cluster at the Fred Hutchinson Cancer Research Center. This research was supported by the National Institute of General Medical Sciences of the NIH under award numbers R00GM107113 and R35GM119835 (A.R.S.). E.K.O. is an Investigator of the Howard Hughes Medical Institute.

AUTHOR CONTRIBUTIONS

Conceptualization, A.M.D., A.R.S., and E.K.O.; Methodology, A.M.D and A.R.S.; Formal Analysis, A.M.D. and A.R.S.; Investigation, A.M.D. and A.R.S.; Writing – Original Draft, A.M.D., A.R.S., and E.K.O.; Writing – Review & Editing, A.M.D., A.R.S., and E.K.O; Funding Acquisition, A.R.S. and E.K.O.; Supervision, A.R.S. and E.K.O.

DECLARATION OF INTERESTS

The authors declare no competing interests.

Received: December 19, 2017
Revised: May 7, 2018
Accepted: June 26, 2018
Published: July 19, 2018

REFERENCES

Alexa, A., and Rahnenfuhrer, J. (2016). topGO: enrichment analysis for gene ontology.

Andreev, D.E., O'Connor, P.B., Fahey, C., Kenny, E.M., Terenin, I.M., Dmitriev, S.E., Cormican, P., Morris, D.W., Shatsky, I.N., and Baranov, P.V. (2015). Translation of 5′ leaders is pervasive in genes resistant to eIF2 repression. eLife *4*, e03971.

Averous, J., Lambert-Langlais, S., Mesclon, F., Carraro, V., Parry, L., Jousse, C., Bruhat, A., Maurin, A.-C., Pierre, P., Proud, C.G., and Fafournoux, P. (2016). GCN2 contributes to mTORC1 inhibition by leucine deprivation through an ATF4 independent mechanism. Sci. Rep. *6*, 27698.

Brandman, O., and Hegde, R.S. (2016). Ribosome-associated protein quality control. Nat. Struct. Mol. Biol. *23*, 7–15.

Buskirk, A.R., and Green, R. (2017). Ribosome pausing, arrest and rescue in bacteria and eukaryotes. Philos. Trans. R. Soc. Lond. B Biol. Sci. *372*, 20160183.

Buttgereit, F., and Brand, M.D. (1995). A hierarchy of ATP-consuming processes in mammalian cells. Biochem. J. *312*, 163–167.

Cerbini, T., Funahashi, R., Luo, Y., Liu, C., Park, K., Rao, M., Malik, N., and Zou, J. (2015). Transcription activator-like effector nuclease (TALEN)-mediated CLYBL targeting enables enhanced transgene expression and one-step generation of dual reporter human induced pluripotent stem cell (iPSC) and neural stem cell (NSC) lines. PLoS ONE *10*, e0116032.

Chan, P.P., and Lowe, T.M. (2016). GtRNAdb 2.0: an expanded database of transfer RNA genes identified in complete and draft genomes. Nucleic Acids Res. *44* (D1), D184–D189.

Chantranupong, L., Scaria, S.M., Saxton, R.A., Gygi, M.P., Shen, K., Wyant, G.A., Wang, T., Harper, J.W., Gygi, S.P., and Sabatini, D.M. (2016). The CASTOR proteins are arginine sensors for the mTORC1 pathway. Cell *165*, 153–164.

Chu, V.T., Weber, T., Wefers, B., Wurst, W., Sander, S., Rajewsky, K., and Kühn, R. (2015). Increasing the efficiency of homology-directed repair for CRISPR-Cas9-induced precise gene editing in mammalian cells. Nat. Biotechnol. *33*, 543–548.

Cong, L., Ran, F.A., Cox, D., Lin, S., Barretto, R., Habib, N., Hsu, P.D., Wu, X., Jiang, W., Marraffini, L.A., and Zhang, F. (2013). Multiplex genome engineering using CRISPR/Cas systems. Science *339*, 819–823.

Dittmar, K.A., Sørensen, M.A., Elf, J., Ehrenberg, M., and Pan, T. (2005). Selective charging of tRNA isoacceptors induced by amino-acid starvation. EMBO Rep. *6*, 151–157.

Doench, J.G., Fusi, N., Sullender, M., Hegde, M., Vaimberg, E.W., Donovan, K.F., Smith, I., Tothova, Z., Wilen, C., Orchard, R., et al. (2016). Optimized sgRNA design to maximize activity and minimize off-target effects of CRISPR-Cas9. Nat. Biotechnol. *34*, 184–191.

Dong, J., Qiu, H., Garcia-Barrio, M., Anderson, J., and Hinnebusch, A.G. (2000). Uncharged tRNA activates GCN2 by displacing the protein kinase moiety from a bipartite tRNA-binding domain. Mol. Cell *6*, 269–279.

Drummond, D.A., and Wilke, C.O. (2008). Mistranslation-induced protein misfolding as a dominant constraint on coding-sequence evolution. Cell *134*, 341–352.

Dunn, J.G., Foo, C.K., Belletier, N.G., Gavis, E.R., and Weissman, J.S. (2013). Ribosome profiling reveals pervasive and regulated stop codon readthrough in Drosophila melanogaster. eLife *2*, e01179.

Elf, J., Nilsson, D., Tenson, T., and Ehrenberg, M. (2003). Selective charging of tRNA isoacceptors explains patterns of codon usage. Science *300*, 1718–1722.

Ferrin, M.A., and Subramaniam, A.R. (2017). Kinetic modeling predicts a stimulatory role for ribosome collisions at elongation stall sites in bacteria. eLife *6*, e23629.

Galtier, N., Roux, C., Rousselle, M., Romiguier, J., Figuet, E., Glémin, S., Bierne, N., and Duret, L. (2018). Codon usage bias in animals: disentangling the effects of natural selection, effective population size, and GC-Biased gene conversion. Mol. Biol. Evol. *35*, 1092–1103.

Gingold, H., Tehler, D., Christoffersen, N.R., Nielsen, M.M., Asmar, F., Kooistra, S.M., Christophersen, N.S., Christensen, L.L., Borre, M., Sørensen, K.D., et al. (2014). A dual program for translation regulation in cellular proliferation and differentiation. Cell *158*, 1281–1292.

Goodarzi, H., Nguyen, H.C.B., Zhang, S., Dill, B.D., Molina, H., and Tavazoie, S.F. (2016). Modulated expression of specific tRNAs drives gene expression and cancer progression. Cell *165*, 1416–1427.

Guydosh, N.R., and Green, R. (2014). Dom34 rescues ribosomes in 3′ untranslated regions. Cell *156*, 950–962.

Han, J., Back, S.H., Hur, J., Lin, Y.-H., Gildersleeve, R., Shan, J., Yuan, C.L., Krokowski, D., Wang, S., Hatzoglou, M., et al. (2013). ER-stress-induced transcriptional regulation increases protein synthesis leading to cell death. Nat. Cell Biol. *15*, 481–490.

Han, K., Jaimovich, A., Dey, G., Ruggero, D., Meyuhas, O., Sonenberg, N., and Meyer, T. (2014). Parallel measurement of dynamic changes in translation rates in single cells. Nat. Methods *11*, 86–93.

Hara, K., Yonezawa, K., Weng, Q.-P., Kozlowski, M.T., Belham, C., and Avruch, J. (1998). Amino acid sufficiency and mTOR regulate p70 S6 kinase and eIF-4E BP1 through a common effector mechanism. J. Biol. Chem. *273*, 14484–14494.

Harding, H.P., Novoa, I., Zhang, Y., Zeng, H., Wek, R., Schapira, M., and Ron, D. (2000). Regulated translation initiation controls stress-induced gene expression in mammalian cells. Mol. Cell *6*, 1099–1108.

Hosios, A.M., Hecht, V.C., Danai, L.V., Johnson, M.O., Rathmell, J.C., Steinhauser, M.L., Manalis, S.R., and Vander Heiden, M.G. (2016). Amino Acids Rather than Glucose Account for the Majority of Cell Mass in Proliferating Mammalian Cells. Dev. Cell *36*, 540–549.

Hsieh, A.C., Liu, Y., Edlind, M.P., Ingolia, N.T., Janes, M.R., Sher, A., Shi, E.Y., Stumpf, C.R., Christensen, C., Bonham, M.J., et al. (2012). The translational landscape of mTOR signalling steers cancer initiation and metastasis. Nature *485*, 55–61.

Ingolia, N.T., Ghaemmaghami, S., Newman, J.R.S., and Weissman, J.S. (2009). Genome-wide analysis in vivo of translation with nucleotide resolution using ribosome profiling. Science *324*, 218–223.

Ingolia, N.T., Lareau, L.F., and Weissman, J.S. (2011). Ribosome profiling of mouse embryonic stem cells reveals the complexity and dynamics of mammalian proteomes. Cell *147*, 789–802.

Ingolia, N.T., Brar, G.A., Rouskin, S., McGeachy, A.M., and Weissman, J.S. (2012). The ribosome profiling strategy for monitoring translation in vivo by deep sequencing of ribosome-protected mRNA fragments. Nat. Protoc. *7*, 1534–1550.

Ishimura, R., Nagy, G., Dotu, I., Zhou, H., Yang, X.-L., Schimmel, P., Senju, S., Nishimura, Y., Chuang, J.H., and Ackerman, S.L. (2014). RNA function. Ribosome stalling induced by mutation of a CNS-specific tRNA causes neurodegeneration. Science *345*, 455–459.

Ishimura, R., Nagy, G., Dotu, I., Chuang, J.H., and Ackerman, S.L. (2016). Activation of GCN2 kinase by ribosome stalling links translation elongation with translation initiation. eLife *5*, e14295.

Jousse, C., Bruhat, A., Ferrara, M., and Fafournoux, P. (2000). Evidence for multiple signaling pathways in the regulation of gene expression by amino acids in human cell lines. J. Nutr. *130*, 1555–1560.

Kimball, S.R. (2002). Regulation of global and specific mRNA translation by amino acids. J. Nutr. *132*, 883–886.

Langmead, B., Trapnell, C., Pop, M., and Salzberg, S.L. (2009). Ultrafast and memory-efficient alignment of short DNA sequences to the human genome. Genome Biol. *10*, R25.

Leprivier, G., Remke, M., Rotblat, B., Dubuc, A., Mateo, A.-R.F., Kool, M., Agnihotri, S., El-Naggar, A., Yu, B., Somasekharan, S.P., et al. (2013). The eEF2 kinase confers resistance to nutrient deprivation by blocking translation elongation. Cell *153*, 1064–1079.

Li, B., and Dewey, C.N. (2011). RSEM: accurate transcript quantification from RNA-Seq data with or without a reference genome. BMC Bioinformatics *12*, 323.

Loayza-Puch, F., Rooijers, K., Buil, L.C.M., Zijlstra, J., Oude Vrielink, J.F., Lopes, R., Ugalde, A.P., van Breugel, P., Hofland, I., Wesseling, J., et al. (2016). Tumour-specific proline vulnerability uncovered by differential ribosome codon reading. Nature *530*, 490–494.

Love, M.I., Huber, W., and Anders, S. (2014). Moderated estimation of fold change and dispersion for RNA-seq data with DESeq2. Genome Biol. *15*, 550.

Mali, P., Yang, L., Esvelt, K.M., Aach, J., Guell, M., DiCarlo, J.E., Norville, J.E., and Church, G.M. (2013). RNA-guided human genome engineering via Cas9. Science *339*, 823–826.

Martin, M. (2011). Cutadapt removes adapter sequences from high-throughput sequencing reads. EMBnet.journal *17*, 10–12.

Nofal, M., Zhang, K., Han, S., and Rabinowitz, J.D. (2017). mTOR inhibition restores amino acid balance in cells dependent on catabolism of extracellular protein. Mol. Cell *67*, 936–946.e5.

Oh, E., Becker, A.H., Sandikci, A., Huber, D., Chaba, R., Gloge, F., Nichols, R.J., Typas, A., Gross, C.A., Kramer, G., et al. (2011). Selective ribosome profiling reveals the cotranslational chaperone action of trigger factor in vivo. Cell *147*, 1295–1308.

Park, Y., Reyna-Neyra, A., Philippe, L., and Thoreen, C.C. (2017). mTORC1 balances cellular amino acid supply with demand for protein synthesis through post-transcriptional control of ATF4. Cell Rep. *19*, 1083–1090.

Presnyak, V., Alhusaini, N., Chen, Y.-H., Martin, S., Morris, N., Kline, N., Olson, S., Weinberg, D., Baker, K.E., Graveley, B.R., and Coller, J. (2015). Codon optimality is a major determinant of mRNA stability. Cell *160*, 1111–1124.

Qian, W., Yang, J.-R., Pearson, N.M., Maclean, C., and Zhang, J. (2012). Balanced codon usage optimizes eukaryotic translational efficiency. PLoS Genet. *8*, e1002603.

Qian, K., Huang, C.T., Chen, H., Blackbourn, L.W., 4th, Chen, Y., Cao, J., Yao, L., Sauvey, C., Du, Z., and Zhang, S.-C. (2014). A simple and efficient system for regulating gene expression in human pluripotent stem cells and derivatives. Stem Cells *32*, 1230–1238.

Rabinovich, S., Adler, L., Yizhak, K., Sarver, A., Silberman, A., Agron, S., Stettner, N., Sun, Q., Brandis, A., Helbling, D., et al. (2015). Diversion of aspartate in ASS1-deficient tumours fosters de novo pyrimidine synthesis. Nature *527*, 379–383.

Radhakrishnan, A., Chen, Y.-H., Martin, S., Alhusaini, N., Green, R., and Coller, J. (2016). The DEAD-box protein Dhh1p couples mRNA decay and translation by monitoring codon optimality. Cell *167*, 122–132.e9.

Ran, F.A., Hsu, P.D., Wright, J., Agarwala, V., Scott, D.A., and Zhang, F. (2013). Genome engineering using the CRISPR-Cas9 system. Nat. Protoc. *8*, 2281–2308.

Reid, D.W., Shenolikar, S., and Nicchitta, C.V. (2015). Simple and inexpensive ribosome profiling analysis of mRNA translation. Methods *91*, 69–74.

Rodriguez, J.M., Maietta, P., Ezkurdia, I., Pietrelli, A., Wesselink, J.-J., Lopez, G., Valencia, A., and Tress, M.L. (2013). APPRIS: annotation of principal and alternative splice isoforms. Nucleic Acids Res. *41*, D110–D117.

Saikia, M., Wang, X., Mao, Y., Wan, J., Pan, T., and Qian, S.-B. (2016). Codon optimality controls differential mRNA translation during amino acid starvation. RNA *22*, 1719–1727.

Sancak, Y., Peterson, T.R., Shaul, Y.D., Lindquist, R.A., Thoreen, C.C., Bar-Peled, L., and Sabatini, D.M. (2008). The Rag GTPases bind raptor and mediate amino acid signaling to mTORC1. Science *320*, 1496–1501.

Saxton, R.A., and Sabatini, D.M. (2017). mTOR signaling in growth, metabolism, and disease. Cell *168*, 960–976.

Schmidt, E.K., Clavarino, G., Ceppi, M., and Pierre, P. (2009). SUnSET, a nonradioactive method to monitor protein synthesis. Nat. Methods *6*, 275–277.

Scott, L., Lamb, J., Smith, S., and Wheatley, D.N. (2000). Single amino acid (arginine) deprivation: rapid and selective death of cultured transformed and malignant cells. Br. J. Cancer *83*, 800–810.

Simms, C.L., Yan, L.L., and Zaher, H.S. (2017). Ribosome Collision Is Critical for Quality Control during No-Go Decay. Mol. Cell *68*, 361–373.

Sonenberg, N., and Hinnebusch, A.G. (2009). Regulation of translation initiation in eukaryotes: mechanisms and biological targets. Cell *136*, 731–745.

Stewart, S.A., Dykxhoorn, D.M., Palliser, D., Mizuno, H., Yu, E.Y., An, D.S., Sabatini, D.M., Chen, I.S.Y., Hahn, W.C., Sharp, P.A., et al. (2003). Lentivirus-delivered stable gene silencing by RNAi in primary cells. RNA *9*, 493–501.

Subramaniam, A.R., Pan, T., and Cluzel, P. (2013a). Environmental perturbations lift the degeneracy of the genetic code to regulate protein levels in bacteria. Proc. Natl. Acad. Sci. USA *110*, 2419–2424.

Subramaniam, A.R., Deloughery, A., Bradshaw, N., Chen, Y., O'Shea, E., Losick, R., and Chai, Y. (2013b). A serine sensor for multicellularity in a bacterium. eLife *2*, e01501.

Subramaniam, A.R., Zid, B.M., and O'Shea, E.K. (2014). An integrated approach reveals regulatory controls on bacterial translation elongation. Cell *159*, 1200–1211.

Supek, F., Bošnjak, M., Škunca, N., and Šmuc, T. (2011). REVIGO summarizes and visualizes long lists of gene ontology terms. PLoS ONE *6*, e21800.

Tang, X., Keenan, M.M., Wu, J., Lin, C.-A., Dubois, L., Thompson, J.W., Freedland, S.J., Murphy, S.K., and Chi, J.-T. (2015). Comprehensive profiling of amino acid response uncovers unique methionine-deprived response dependent on intact creatine biosynthesis. PLoS Genet. *11*, e1005158.

Thoreen, C.C., Kang, S.A., Chang, J.W., Liu, Q., Zhang, J., Gao, Y., Reichling, L.J., Sim, T., Sabatini, D.M., and Gray, N.S. (2009). An ATP-competitive mammalian target of rapamycin inhibitor reveals rapamycin-resistant functions of mTORC1. J. Biol. Chem. *284*, 8023–8032.

Thoreen, C.C., Chantranupong, L., Keys, H.R., Wang, T., Gray, N.S., and Sabatini, D.M. (2012). A unifying model for mTORC1-mediated regulation of mRNA translation. Nature *485*, 109–113.

Vander Heiden, M.G., and DeBerardinis, R.J. (2017). Understanding the intersections between metabolism and cancer biology. Cell *168*, 657–669.

Varshney, U., Lee, C.P., and RajBhandary, U.L. (1991). Direct analysis of aminoacylation levels of tRNAs in vivo. Application to studying recognition of Escherichia coli initiator tRNA mutants by glutaminyl-tRNA synthetase. J. Biol. Chem. *266*, 24712–24718.

Wang, S., Tsun, Z.-Y., Wolfson, R.L., Shen, K., Wyant, G.A., Plovanich, M.E., Yuan, E.D., Jones, T.D., Chantranupong, L., Comb, W., et al. (2015). Metabolism. Lysosomal amino acid transporter SLC38A9 signals arginine sufficiency to mTORC1. Science *347*, 188–194.

Wolfson, R.L., Chantranupong, L., Saxton, R.A., Shen, K., Scaria, S.M., Cantor, J.R., and Sabatini, D.M. (2016). Sestrin2 is a leucine sensor for the mTORC1 pathway. Science *351*, 43–48.

Ye, J., Kumanova, M., Hart, L.S., Sloane, K., Zhang, H., De Panis, D.N., Bobrovnikova-Marjon, E., Diehl, J.A., Ron, D., and Koumenis, C. (2010). The GCN2-ATF4 pathway is critical for tumour cell survival and proliferation in response to nutrient deprivation. EMBO J. *29*, 2082–2096.

Zaborske, J.M., Wu, X., Wek, R.C., and Pan, T. (2010). Selective control of amino acid metabolism by the GCN2 eIF2 kinase pathway in Saccharomyces cerevisiae. BMC Biochem. *11*, 29.

Zhang, P., McGrath, B.C., Reinert, J., Olsen, D.S., Lei, L., Gill, S., Wek, S.A., Vattem, K.M., Wek, R.C., Kimball, S.R., et al. (2002). The GCN2 eIF2α kinase is required for adaptation to amino acid deprivation in mice. Mol. Cell. Biol. *22*, 6681–6688.

Zid, B.M., and O'Shea, E.K. (2014). Promoter sequences direct cytoplasmic localization and translation of mRNAs during starvation in yeast. Nature *514*, 117–121.

STAR★METHODS

KEY RESOURCES TABLE

REAGENT or RESOURCE	SOURCE	IDENTIFIER
Antibodies		
Rabbit polyclonal anti GCN2	Cell Signaling Technology (CST)	3302S; RRID:AB_10694800
Rabbit polyclonal anti eEF2K	CST	3692S; RRID:AB_10694413
Rabbit polyclonal anti EEF2	CST	2332S; RRID:AB_10693546
Rabbit polyclonal anti P∼T56 EEF2	CST	2331S; RRID:AB_10015204
Rabbit monoclonal anti eIF2α	CST	5324P; RRID:AB_10692650
Rabbit monoclonal anti P∼S51 eIF2α	CST	3398P; RRID:AB_2096481
Rabbit polyclonal anti S6K	CST	9202S; RRID:AB_331676
Rabbit polyclonal anti P∼T389 S6K	CST	9205S; RRID:AB_330944
Rabbit monoclonal anti S6 ribosomal protein (RPS6)	CST	2217S; RRID:AB_331355
Rabbit monoclonal anti P∼S235/6 RPS6	CST	4858S; RRID:AB_916156
Rabbit monoclonal anti GAPDH	CST	2118S; RRID:AB_561053
Rabbit monoclonal anti puromycin	Sigma-Aldrich	MABE343; RRID:AB_2566826
Mouse monoclonal anti FLAG	Sigma-Aldrich	F3165; RRID:AB_259529
Goat polyclonal anti rabbit IgG, HRP-linked	CST	7074S; RRID:AB_2099233
Goat polyclonal anti mouse IgG, HRP-linked	Sigma-Aldrich	12-349; RRID:AB_390192
Chemicals, Peptides, and Recombinant Proteins		
High-glucose DMEM without pyruvate	GIBCO	11995065
Fetal bovine serum	ATCC	30-2020
Low glucose DMEM powder without amino acids	US Bio	D9800-13
Dialyzed FBS	Invitrogen	26400-044
Lipofectamine 3000	Thermo Fisher Scientific (TFS)	L3000015
Cycloheximide	Sigma-Aldrich	C7698-1G
Turbo DNase	TFS	AM2238
Micrococcal nuclease	Worthington Biochemical	LS004798
SYBR gold nucleic acid gel stain	TFS	S11494
Superase-In RNase inhibitor	TFS	AM2696
T4 PNK	NEB	M0201S
E. coli poly A polymerase	NEB	M0276S
Superscript III	TFS	18080093
Circligase	Epicenter	CL4111K
Acid-Phenol:Chloroform pH 4.5 with isoamyl alcohol at 25:24:1	TFS	AM9720
MyOne Streptavidin Dynabeads	TFS	65001
Phusion Flash High-Fidelity PCR master mix	TFS	F548S
RNase I	Invitrogen	AM2294
Sequagel Urea gel system	National Diagnostics	EC-833
BSA	CST	9998S
SuperSignal West Femto Substrate	TFS	34095
Restore Western Blot stripping buffer	TFS	21059
PerfectHyb Plus Hybridization buffer	Sigma-Aldrich	H-7033
[γ-P^{32}]-ATP EasyTide	Perkin Elmer	NEG502A250UC
Puromycin	Sigma-Aldrich	P8833
dT-20 primer	TFS	18418020

(*Continued on next page*)

Continued

REAGENT or RESOURCE	SOURCE	IDENTIFIER
PowerUp SYBR Green PCR master mix	TFS	A25742
Glycoblue	TFS	AM9516
Critical Commercial Assays		
CellTiter-Glo	Promega	G7570
Quick RNA Miniprep	Zymo	R1054
Deposited Data		
Ribosome profiling	this study	GEO: GSE113751
Raw/processed data on Github	this study	https://github.com/rasilab/adarnell_2018
Experimental Models: Cell Lines		
HEK293T	ATCC	CRL-3216
HeLa	ATCC	CCL2
HCT116	NIH, National Cancer Institute (NCI)	NCI-60 cancer cell line panel
hsAD1: HEK293T AAVS1-hrGFP	Donor pADHS1, targeting pADHS4	N/A
hsAD2: HEK293T AAVS1-RagB-WT	Donor pADHS2, targeting pADHS4	N/A
hsAD3: HEK293T AAVS1-RagB-Q99L	Donor pADHS3, targeting pADHS4	N/A
hsAD4: HEK293T GCN2 KO (clones 1,2,3)	Targeting pADHS7,8	N/A
hsAD5: HEK293T EEF2K KO (clones 1,4,5)	Targeting pADHS9,10	N/A
hsAD6: HEK293T YFP-CGC	Donor pADHS15, pack/env pADHS11,12	N/A
hsAD7: HEK293T YFP-CGG	Donor pADHS16, pack/env pADHS11,12	N/A
hsAD8: HEK293T YFP-CGA	Donor pADHS17, pack/env pADHS11,12	N/A
hsAD9:: HEK293T YFP-CGU	Donor pADHS18, pack/env pADHS11,12	N/A
hsAD10: HEK293T YFP-AGA	Donor pADHS19, pack/env pADHS11,12	N/A
hsAD11: HEK293T YFP-AGG	Donor pADHS20, pack/env pADHS11,12	N/A
hsAD12: HEK293T GCN2 KO YFP-CGC	Donor pADHS15, pack/env pADHS11,12	N/A
hsAD13: HEK293T GCN2 KO YFP-CGG	Donor pADHS16, pack/env pADHS11,12	N/A
hsAD14: HEK293T GCN2 KO YFP-CGA	Donor pADHS17, pack/env pADHS11,12	N/A
hsAD15: HEK293T GCN2 KO YFP-CGU	Donor pADHS18, pack/env pADHS11,12	N/A
hsAD16: HEK293T GCN2 KO YFP-AGA	Donor pADHS19, pack/env pADHS11,12	N/A
hsAD17: HEK293T GCN2 KO YFP-AGG	Donor pADHS20, pack/env pADHS11,12	N/A
hsAD18: HEK293T YFP-CUA	Donor pADHS21, pack/env pADHS11,12	N/A
hsAD19: HEK293T YFP-CUC	Donor pADHS22, pack/env pADHS11,12	N/A
hsAD20: HEK293T YFP-CUU	Donor pADHS23, pack/env pADHS11,12	N/A
hsAD21: HEK293T YFP-UUA	Donor pADHS24, pack/env pADHS11,12	N/A
hsAD22: HEK293T YFP-UUG	Donor pADHS25, pack/env pADHS11,12	N/A

(*Continued on next page*)

Continued

REAGENT or RESOURCE	SOURCE	IDENTIFIER
hsAD23: HEK293T GCN2 KO YFP-CUA	Donor pADHS21, pack/env pADHS11,12	N/A
hsAD24: HEK293T GCN2 KO YFP-CUC	Donor pADHS22, pack/env pADHS11,12	N/A
hsAD25: HEK293T GCN2 KO YFP-CUU	Donor pADHS23, pack/env pADHS11,12	N/A
hsAD26: HEK293T GCN2 KO YFP-UUA	Donor pADHS24, pack/env pADHS11,12	N/A
hsAD27: HEK293T GCN2 KO YFP-UUG	Donor pADHS25, pack/env pADHS11,12	N/A
hsAD28: HEK293T UUG8	Donor pADHS26, pack/env pADHS11,12	N/A
hsAD29: HEK293T CUA8	Donor pADHS27, pack/env pADHS11,12	N/A
hsAD30: HEK293T GCN2 KO UUG8	Donor pADHS26, pack/env pADHS11,12	N/A
hsAD31: HEK293T GCN2 KO CUA8	Donor pADHS27, pack/env pADHS11,12	N/A
hsAD32: HEK293T CUA4UUG4	Donor pADHS28, pack/env pADHS11,12	N/A
hsAD33: HEK293T CUA6UUG2	Donor pADHS29, pack/env pADHS11,12	N/A
hsAD34: HEK293T GCN2 KO CUA4UUG4	Donor pADHS28, pack/env pADHS11,12	N/A
hsAD35: HEK293T GCN2 KO CUA6UUG2	Donor pADHS29, pack/env pADHS11,12	N/A
hsAD39: HEK293T pAAVS1P-iCAG.FlagYFP-DHFR-CGC	Donor pADHS34, targeting pADHS4	N/A
hsAD40: HEK293T pAAVS1P-iCAG.FlagYFP-DHFR-CGG	Donor pADHS35, targeting pADHS4	N/A
hsAD41: HCT116 pAAVS1P-iCAG.FlagYFP-DHFR-CGC	Donor pADHS34, targeting pADHS4	N/A
hsAD42: HCT116 pAAVS1P-iCAG.FlagYFP-DHFR-CGG	Donor pADHS34, targeting pADHS4	N/A
hsAD43: HCT116 YFP-CGC	Donor pADHS15, pack/env pADHS11,12	N/A
hsAD44: HCT116 YFP-CGG	Donor pADHS16, pack/env pADHS11,12	N/A
hsAD45: HeLa YFP-CGC	Donor pADHS15, pack/env pADHS11,12	N/A
hsAD46: HeLa YFP-CGG	Donor pADHS16, pack/env pADHS11,12	N/A
Oligonucleotides		
tRNA Northern blot probe, Arg-ACG1: CCAGGAGTCGA ACCTRGAATCTTCTGATCCGTAGTCAGACGCG	this study	N/A
tRNA Northern blot probe, Arg-CCG3: ACTCGAA CCCTCAATCTTCTGATCCGGAATCAGACGCCTT	this study	N/A
tRNA Northern blot probe, Arg-TCG2: GGATTCGA ACCCTCAATCTTCTGATCCGAAGTCAGACGCC	this study	N/A
tRNA Northern blot probe, Leu-TAG3: AAGAGACTGG AGCCTAAATCCAGCGCCTTAGACCGCTCGGC CACACTACC	this study	N/A
tRNA Northern blot probe, Leu-AAG3: AGTCTTAAT ACAGTGCCTTAGACCGCTCGGCCACCCTACC	this study	N/A

(*Continued on next page*)

Continued

REAGENT or RESOURCE	SOURCE	IDENTIFIER
tRNA Northern blot probe, Leu-CAG2: CACGCCTC CAGGGGAGACTGCGACCTGAACGCAGCGCCTT	this study	N/A
tRNA Northern blot probe, Leu-CAA5: CCACGCC TCCATTGGAGACCACAAGCTTGAGTCTGGCGCC	this study	N/A
o3285_123:154_rp rRNA subtraction oligo: [Biotin-5] CCTCCCGGGGCTACGCCTGTCTGAGCGTCGC	this study	N/A
o3287_4990:5022_rp rRNA subtraction oligo: [Biotin-5]TCGCTGCGATCTATTGAAAGTCAGC CCTCGAC	this study	N/A
YFP-DHFR reporter qPCR primer F (to DHFR C terminus): ATATCGACGCAGAAGTGGAAGG	this study	N/A
YFP-DHFR reporter qPCR primer R (to DHFR C terminus): ATCAGCATCGTGGAATTCGC	this study	N/A
Premature termination reporter qPCR primer F (spans tandem Leucine codons): GAGTTCGTGA CCGCCGC	this study	N/A
Premature termination reporter qPCR primer R (spans tandem Leucine codons): CCATGCC GATAACGTGATCTACCG	this study	N/A
Homologous recombination at AAVS1 locus PCR check, F (in AAVS1 locus): CTCTCTCCTGAGTC CGGACCACTTTGAGCTC	this study	N/A
Homologous recombination at AAVS1 locus PCR check, R (in puroR): CGCACCGTGGGCTTGTA CTCGGTCAT	this study	N/A
Recombinant DNA		
pADHS1: AAVS1-CAG-hrGFP	Qian et al., 2014	Addgene #52344
pADHS2: AAVS1-CAG-RagBWT	Cloned from Qian et al., 2014 and Sancak et al., 2008	Cloned Flag-RagB-WT from Flag pLJM1 RagB wt, Addgene #19313, into AAVS1-CAG-hrGFP
pADHS3: AAVS1-CAG-RagBQ99L	Cloned from Qian et al., 2014 and Sancak et al., 2008	Cloned Flag-RagB-Q99L from Flag pLJM1 RagB 99L, Addgene #19315, into AAVS1-CAG-hrGFP
pADHS4: px330-AAVS1-T2	Cloned from Cong et al., 2013	Cloned AAVS1 T2 guide sequence in px330-U6-Chimeric-BB-CBh-hSpCas9, Addgene #42230
pADHS5: pU6-(BbsI)_CBh-Cas9-T2A-BFP	Chu et al., 2015	Addgene #64323
pADHS6: pSpCas9(BB)-2A-GFP (PX458)	Ran et al., 2013	Addgene #48138
pADHS7: pU6-GCN2-1-Cas9-2A-BFP	Cloned from Chu et al., 2015	Cloned GCN2 (EIF2AK4) guide RNA sequence 2 (Doench et al., 2016, Addgene #75876) into pU6-(BbsI)_ CBh-Cas9-T2A-BFP
pADHS8: pU6-GCN2-2-Cas9-2A-GFP	Cloned from Ran et al., 2013	Cloned GCN2 (EIF2AK4) guide RNA sequence 3 (Doench et al., 2016, Addgene #75877) into pSpCas9(BB)-2A-GFP (PX458)
pADHS9: pU6-EEF2K-1-Cas9-2A-BFP	Cloned from Chu et al., 2015	Cloned EEF2K guide RNA sequence 2 (Doench et al., 2016, Addgene #77855) into pU6-(BbsI)_CBh-Cas9-T2A-BFP
pADHS10: pU6-EEF2K-2-Cas9-2A-GFP	Cloned from Ran et al., 2013	Cloned EEF2K guide RNA sequence 3 (Doench et al., 2016, Addgene #77856) into pU6-EEF2K-2-Cas9-2A-GFP
pADHS11: psPAX2	N/A	Addgene #12260
pADHS12: pCMV-VSV-G	Stewart et al., 2003	Addgene #8454

(*Continued on next page*)

Continued

REAGENT or RESOURCE	SOURCE	IDENTIFIER
pADHS13: pLJM1-EGFP	Sancak et al., 2008	Addgene #19319
pADHS14: KHT61-Unreg-YFP-DD	Han et al., 2014	A gift from Kyuho Han
pADHS15: pLJM1-Flag-YFP-DHFR (YFP-CGC)	Cloned from Sancak et al., 2008 and Han et al., 2014	Cloned YFP-DD from KHT61-Unreg-YFP-DD into pLJM1-EGFP with a Flag Tag
pADHS16: pLJM1-Flag-YFP-DHFR (YFP-CGG)	Cloned from YFP-CGC	Cloned 2 gBlocks with all YFP and DHFR arginine codons swapped to CGG into YFP-CGC
pADHS17: pLJM1-Flag-YFP-DHFR (YFP-CGA)	Cloned from YFP-CGC	Cloned 2 gBlocks with all YFP and DHFR arginine codons swapped to CGA into YFP-CGC
pADHS18: pLJM1-Flag-YFP-DHFR (YFP-CGU)	Cloned from YFP-CGC	Cloned 2 gBlocks with all YFP and DHFR arginine codons swapped to CGU into YFP-CGC
pADHS19: pLJM1-Flag-YFP-DHFR (YFP-AGA)	Cloned from YFP-CGC	Cloned 2 gBlocks with all YFP and DHFR arginine codons swapped to AGA into YFP-CGC
pADHS20: pLJM1-Flag-YFP-DHFR (YFP-AGG)	Cloned from YFP-CGC	Cloned 2 gBlocks with all YFP and DHFR arginine codons swapped to AGG into YFP-CGC
pADHS21: pLJM1-Flag-YFP-DHFR (YFP-CUA)	Cloned from YFP-CGC	Cloned 1 gBlock with all YFP leucine codons swapped to CUA into YFP-CGC
pADHS22: pLJM1-Flag-YFP-DHFR (YFP-CUC)	Cloned from YFP-CGC	Cloned 1 gBlock with all YFP leucine codons swapped to CUC into YFP-CGC
pADHS23: pLJM1-Flag-YFP-DHFR (YFP-CUU)	Cloned from YFP-CGC	Cloned 1 gBlock with all YFP leucine codons swapped to CUU into YFP-CGC
pADHS24: pLJM1-Flag-YFP-DHFR (YFP-UUA)	Cloned from YFP-CGC	Cloned 1 gBlock with all YFP leucine codons swapped to UUA into YFP-CGC
pADHS25: pLJM1-Flag-YFP-DHFR (YFP-UUG)	Cloned from YFP-CGC	Cloned 1 gBlock with all YFP leucine codons swapped to UUG into YFP-CUA
pADHS26: pLJM1-Flag-YFP-UUG8-DHFR (UUG8)	Cloned from YFP-CUA	Cloned 8 tandem UUG codons into YFP-CUA
pADHS27: pLJM1-Flag-YFP-CUA8-DHFR (CUA8)	Cloned from YFP-CUA	Cloned 8 tandem CUA codons into YFP-CUA
pADHS28: pLJM1-Flag-YFP-CUA4UUG4-DHFR (CUA4UUG4)	Cloned from YFP-CUA	Cloned UUG-CUA-UUG-CUA-UUG-CUA-UUG-CUA into YFP-CUA
pADHS29: pLJM1-Flag-YFP-CUA6UUG2-DHFR (CUA6UUG2)	Cloned from YFP-CUA	Cloned CUA-CUA-UUG-CUA-CUA-UUG-CUA-CUA into YFP-CUA
pADHS33: pAAVS1P-iCAG.copGFP	Cerbini et al., 2015	Addgene #66577
pADHS34: pAAVS1P-iCAG.FlagYFP-DHFR-CGC	Cloned from Cerbini et al., 2015 and YFP-CGC	Cloned YFP-DHFR from YFP-CGC into pAAVS1P-iCAG.copGFP
pADHS35: pAAVS1P-iCAG.FlagYFP-DHFR-CGG	Cloned from Cerbini et al., 2015 and YFP-CGG	Cloned YFP-DHFR from YFP-CGG into pAAVS1P-iCAG.copGFP
Software and Algorithms		
cutadapt	Martin, 2011	N/A
bowtie	Langmead et al., 2009	N/A
rsem	Li and Dewey, 2011	N/A
DESeq2	Love et al., 2014	N/A
topGO	Alexa and Rahnenfuhrer, 2016	N/A
REVIGO	Supek et al., 2011	N/A

CONTACT FOR REAGENT AND RESOURCE SHARING

Further information and requests for resources and reagents should be directed to and will be fulfilled by the Lead Contact, Arvind Subramaniam (rasi@fredhutch.org).

EXPERIMENTAL MODEL AND SUBJECT DETAILS

See Key Resources Table for catalog numbers for commercial reagents.

Human cell line culture

The HEK293T (RRID:CVCL_0063) and HeLa cell lines (RRID:CVCL_0030) were obtained from ATCC, catalog numbers CRL-3216 and CCL-2. The HCT116 cell line (RRID:CVCL_0291) was obtained from the National Cancer Institute (NCI) panel of 60 cancer lines. Cells lines from ATCC and the NCI-60 panel are authenticated. All cell lines were passaged in high-glucose DMEM without pyruvate, with penicillin/streptomycin, and with 10% fetal bovine serum at 37°C and 5% CO_2. The HEK293T cell line, used as the primary model and parental cell line for CRISPR/lentiviral genome editing in the paper, and the HCT116 cell line tested negative for mycoplasma contamination. The HeLa cell line was not tested, but all experiments were performed with low passage number stocks from ATCC.

Limitation for single amino acids

Amino acid limitation media were prepared from low glucose DMEM powder without amino acids; all amino acids except leucine and arginine, and glucose were supplemented according to this recipe: 3 g/L additional glucose, 30 mg/L glycine, 63 mg/L cysteine 2·HCl, 580 mg/L glutamine, 42 mg/L histidine HCl·H_2O, 105 mg/L isoleucine, 146 mg/L lysine HCl, 30 mg/L methionine, 66 mg/L phenylalanine, 42 mg/L serine, 95 mg/L threonine, 16 mg/L tryptophan, 64 mg/L tyrosine 2·Na 2·H_2O, and 94 mg/L valine. Medium was prepared in batches of 2 l; the pH was adjusted to 7.2–7.4 with HCl, and medium was vacuum filtered and supplemented with 10% dialyzed FBS. For all amino acid limitation assays—except time course experiments over multiple days—cells were expanded to 60%–70% confluency in amino acid limitation medium supplemented with 105 mg/L leucine and 84 mg/L arginine HCl. Cells were then washed once in PBS and transferred to limitation medium supplemented with either 105 mg/L leucine (for arginine limitation) or 84 mg/L arginine HCl (for leucine limitation), or both (for rich medium). To account for different proliferation rates for cells in the rich and amino acid limited conditions in time course experiments over multiple days, cells for the rich medium condition were expanded to 10%–20% confluency and cells for the leucine / arginine limitation conditions were expanded to 60%–70% confluency in the same arginine and leucine supplemented amino acid limitation medium before beginning the experiment.

METHOD DETAILS

See Key Resources Table for catalog numbers for commercial reagents. Unless otherwise indicated, commercial reagents were used according to the manufacturer's instructions.

Construction of plasmids

AAVS1-CAG-hrGFP was from Su-Chun Zhang (Addgene # 52344) (Qian et al., 2014). We cloned sequences for FLAG-RagB-WT and FLAG-RagB-Q99L into this plasmid in place of hrGFP, from sequences in FLAG pLJM1 RagB WT (Addgene # 19313) and FLAG pLJM1 RagB 99L (Addgene # 19315) from David Sabatini (Sancak et al., 2008). The resulting CRISPR homology donor plasmids AAVS1-CAG-hrGFP (pADHS1), AAVS1-CAG-RagBWT (pADHS2), and AAVS1-CAG-RagBQ99L (pADHS3) were then introduced into HEK293T cells (see Figure 4C) by CRISPR/Cas9 mediated homologous recombination with the AAVS1 sgRNA and Cas9 expression plasmid px330-AAVS1-T2 (pADHS4), which was cloned by inserting the AAVS1-T2 target sequence GGGGCCACTAGGGA CAGGAT (Mali et al., 2013) into the px330-U6-Chimeric-BB-CBh-hSpCas9 plasmid, from Feng Zhang (Addgene # 42230) (Cong et al., 2013).

To generate plasmids for targeting endogenous GCN2 (alias EIF2AK4) and EEF2K (see Figures S4G and S5D), sgRNA sequences were obtained from the lentiGuide-Puro library (Doench et al., 2016). Two sgRNA sequences each targeting exonic sequences ~790 bp apart in GCN2 (from Addgene #75876 and 75877), and ~230 bp apart in EEF2K (from Addgene #77855 and 77856), were selected. For each pair, one sgRNA was cloned into pU6-(BbsI)_CBh-Cas9-T2A-BFP (pADHS5), from Ralf Kuehn (Addgene # 64323) (Chu et al., 2015), and the other into pSpCas9(BB)-2A-GFP (PX458) (pADHS6), from Feng Zhang (Addgene # 48138) (Ran et al., 2013). This produced the targeting plasmids pU6-GCN2-1-Cas9-2A-BFP (pADHS7), pU6-GCN2-2-Cas9-2A-GFP (pADHS8), pU6-EEF2K-1-Cas9-2A-BFP (pADHS9), and pU6-EEF2K-2-Cas9-2A-GFP (pADHS10) (see CRISPR/Cas9 genome editing, KO section).

Our YFP-DHFR protein synthesis rate reporters (see Figure 6A) were cloned into pLJM1-EGFP, from David Sabatini (Addgene # 19319) (Sancak et al., 2008) (pADHS13). The EGFP coding sequence in this vector was replaced by the YFP-DHFR sequence from KHT61-Unreg-YFP-DD, a gift from Kyuho Han (Han et al., 2014) (pADHS14), along with an N-terminal FLAG tag to generate the pLJM1-FLAG-YFP-DHFR reporter (YFP-CGC, pADHS15). The YFP-CGC reporter has 13 CGC and 1 CGU arginine codons, and 23 CUG, 5 CUC, 2 UUA, and 2 UUG leucine codons. To generate codon variants, gBlocks (IDT) were ordered in which all 14 arginine

codons in YFP and DHFR, or all 21 leucine codons in YFP, were swapped to one out of each of the six synonymous leucine or arginine codons; these gBlocks were cloned in place of the YFP-CGC sequence in the pLJM1 plasmid backbone. The following library of FLAG-tagged codon variant reporter lentiviral donor plasmids was generated: YFP-CGC (pADHS15), YFP-CGG (pADHS16), YFP-CGA (pADHS17), YFP-CGU (pADHS18), YFP-AGA (pADHS19), YFP-AGG (pADHS20), YFP-CUA (pADHS21), YFP-CUC (pADHS22), YFP-CUU (pADHS23), YFP-UUA (pADHS24), and YFP-UUG (pADHS25) (see Lentiviral transduction, overexpression section).

These reporters were modified to generate premature termination reporters (see Figure 6F) by cloning in eight tandem leucine codons into the pLJM1-YFP-CUA (pADHS21) lentiviral donor plasmid in between the YFP and DHFR sequences. The following library of four FLAG-tagged premature termination reporter lentiviral donor plasmids was generated, in which the numbers refer to the composition of the eight leucine codon repeat: UUG8 (pADHS26), CUA8 (pADHS27), CUA4UUG4 (pADHS28), CUA6UUG2 (pADHS29). These plasmids were used to generate stable reporter cell lines by lentiviral transduction into HEK293T and the HEK293T GCN2 KO cell line (see Lentiviral transduction, overexpression section).

A variant YFP-DHFR protein synthesis rate reporter (see Figure S6C) was built by cloning from pAAVS1P-iCAG.copGFP, from Jizhong Zou (Addgene # 66577) (Cerbini et al., 2015) (pADHS33). To generate pAAVS1P-iCAG.FLAG-YFP-DHFR-CGC (pADHS34) and -CGG (pADHS35) codon variant reporters, reporter sequences from YFP-CGC and YFP-CGG were cloned in place of copGFP. These plasmids were used to generate stable reporter cell lines in HEK293T and HCT116 cells by CRISPR/Cas9-mediated homologous recombination with px330-AAVS1-T2 (see CRISPR/Cas9 genome editing, overexpression section).

Stable cell line generation

All transfections were performed at 75% confluency using Lipofectamine 3000. Selection was performed with puromycin: 2 μg/mL for HEK293T cells, 1 μg/mL for HCT116/HeLa cells.

Lentiviral transduction, overexpression

HEK293T cells were transfected in a 10 cm plate with donor expression plasmid pLJM1 containing the desired insert, psPAX2, from Didier Trono (Addgene # 12260) (pADHS11), and pCMV-VSV-G, from Bob Weinberg (Addgene # 8454) (Stewart et al., 2003) (pADHS12) in a 10:9:1 ratio (by weight). The medium was replaced after 12-16 hr, and lentivirus was harvested at 48 hr by passing culture supernatant through a low-protein binding filter with 0.45 μm pore size. 1 mL of virus was then used to transduce 50%–60% confluent HEK293T, HeLa, or HCT116 cells in a 6 cm plate. Transduced cells were passaged to a 10 cm plate after 24 hr, and puromycin selection was initiated after 48 hr (see Figures 6B–6E and S6A–S6C).

CRISPR/Cas9 genome editing, overexpression

To generate hrGFP, RagB-WT, and RagB-Q99L cell lines (see Figure 4C): HEK293T cells in a 6-well plate were transfected with homology donor plasmid (pAAVS1-CAG-hrGFP, pAAVS1-CAG-RagBWT, or pAAVS1-CAG-RagBQ99L) and px330-AAVS1-T2 at a ratio of 4:1 (2 μg donor: 500 ng guide). Homologous recombination and expression of transgenes were confirmed in the resulting polyclonal population by PCR, flow cytometry, and western blotting after puromycin selection.

To generate arginine/leucine codon variant YFP-DHFR reporter cells lines (see Figure S6B): HEK293T or HCT116 cells were transfected with homology donor plasmid (for YFP reporter lines: pAAVS1P-iCAG.copGFP, pAAVS1P-iCAG.FLAG-YFP-DHFR-CGC, pAAVS1P-iCAG.FLAG-YFP-DHFR-CGG) and px330-AAVS1-T2 at a ratio of 2:1 (10 μg donor: 5 μg guide). Homologous recombination and TMP-inducible YFP fluorescence were confirmed in the resulting polyclonal population by PCR, flow cytometry, and western blotting after puromycin selection.

CRISPR/Cas9 genome editing, KO

HEK293T cells in a 12-well plate were transfected with 500 ng of each targeting plasmid, in the following four combinations: (1) both pU6-GCN2-1-Cas9-2A-BFP and pU6-GCN2-2-Cas9-2A-GFP, (2) both pU6-EEF2K-1-Cas9-2A-BFP and pU6-EEF2K-2-Cas9-2A-GFP, (3) pU6-GCN2-1-Cas9-2A-BFP only, and (4) pU6-GCN2-2-Cas9-2A-GFP only. Cells were transferred to a 6-well plate 24 hr post transfection. After 48 hr, dual-fluorescing BFP+ and GFP+ single cells were sorted into individual wells of a 96-well plate; samples 3 and 4 were used to define individual gates. Plates were spun at 100 *g*, 1 min to sediment cells. After expansion, western blotting confirmed complete KO. 92% of clones tested were positive for complete GCN2 KO (11/12), and 83% for EEF2K KO (10/12) (see Figures S4G and S5D).

Ribosome profiling

To detect codon-specific ribosome pausing, ribosome profiling was performed according to (Ingolia et al., 2009), with modifications detailed below (see Figures 1, 4, S1, and S4).

Cells were expanded to 75% confluency in two 15 cm plates. Cells were washed once, briefly, in ice cold PBS. PBS was thoroughly drained, and plates were immersed in liquid nitrogen for flash freezing and then transferred to –80°C. Frozen cells were lysed on each plate by scraping into 300 μL lysis buffer (20 mM Tris pH 7.5, 15 mM $MgCl_2$, 150 mM NaCl, 100 μg/mL cycloheximide, 5 mM $CaCl_2$, 1% Triton X-100, 50 U/mL Turbo DNase), and lysates from the two 15 cm plates were combined to yield ~1 mL of lysate. Ribosome footprints were generated from 450 μL of lysate by 1 hr of digestion with 800 U micrococcal nuclease at room temperature (25°C) with nutation, and quenched by addition of 4.5 μL 0.5 M EGTA. Footprints were purified by sucrose density gradient fractionation; a BioComp Gradient Station was used to generate 10%–50% sucrose density gradients in 1X polysome resuspension buffer (20 mM Tris pH 7.5, 15 mM $MgCl_2$, 150 mM NaCl, 100 μg/mL cycloheximide). 400 μL digested lysate was loaded onto gradients in SW41 rotor buckets and samples were spun for 2.5 hr at 35,000 RPM and 4°C. Fractionation was performed at 0.22 mm/s with

UV absorbance monitoring at 254 nm (EconoUV Monitor), and the monosome fraction was collected in addition to the contiguous disome "shoulder." Total RNA was purified by addition of 7 mM EDTA and 1% SDS, extraction in acid-phenol:chloroform pH 4.5 with isoamyl alcohol at 25:24:1 at 65°C, and precipitated.

8 μg of the monosome fraction RNA was run on a 15% TBE-urea gel (Bio-Rad) and footprints were excised from ~26-40 nt (see Figure S1D). RNA was extracted in 0.3 M NaOAc pH 5.5, 1 mM EDTA, and 100 U/mL Superase-In overnight at room temperature with rotating and then precipitated.

Footprints were dephosphorylated with T4 PNK, then precipitated. Footprints were then polyA-tailed with *E. coli* polyA polymerase for 10 min, then precipitated. Reverse transcription was performed using SuperScript III and 0.5 μM oTi19pA oligo primer (Zid and O'Shea, 2014) for 30 min at 48°C, RT products were run on a 10% TBE-urea gel (Bio-Rad), extracted from gel slices and precipitated. RT products were circularized with CircLigase, then precipitated. rRNA was removed by subtractive hybridization with MyOne Streptavidin Dynabeads. Two biotinylated reverse complement oligos to discrete rRNA sequences that were recovered extremely abundantly in our test ribosome profiling libraries (o3285, o3287; used in a 1:3 ratio) were annealed to circularized libraries, and an equal volume of washed beads was added to annealed oligo/libraries for 15 min at 37°C. Supernatant was recovered and precipitated. Resulting libraries were amplified by 6-12 cycles of PCR with 2X Phusion Flash master mix with common reverse and unique 6nt index forward library primers and purified after running on a 10% TBE gel (Bio-Rad). Libraries were extracted from gel slices, precipitated, resuspended in 10 μL Tris 10 mM pH 7, and quantified using an Agilent TapeStation or Bioanalyzer. Up to 15 multiplexed libraries were submitted for sequencing on both lanes of an Illumina HiSeq 2500 Rapid Flow Cell. Sequencing runs yielded approximately 150 million reads per lane.

Notably, two ribonucleases, RNase I and micrococcal nuclease (MNase), are commonly used for ribosome profiling. We observed near-complete degradation of the 60S ribosomal subunit and ribosome-bound mRNA fractions by RNase I in buffers with either high (Ingolia et al., 2012) or low magnesium (Andreev et al., 2015) and across a broad range of RNase I concentrations (Figures S1A and S1B). The 60S and monosome fractions were largely intact after digestion with MNase (Figure S1C), and therefore we used this nuclease. As previously reported (Dunn et al., 2013; Reid et al., 2015), MNase results in slightly longer reads and a broader read length distribution (Figure S1E) as it does not digest completely around bound ribosomes. However, read density exhibited three nucleotide periodicity, is clearly enriched in the coding region, and exhibits peaks at start and stop codons (Figures S1F and S1G), allowing resolution of codon-level changes in translation elongation.

Polysome profiling

The same procedure as in the "Ribosome profiling" section was used, with the following modifications. 150 μL of clarified lysate was loaded directly onto sucrose density gradients. Gradients were centrifuged in a SW41 rotor at 35,000 RPM for 3 hr at 4°C with the "slow" brake setting. After fractionation, the relative polysome to monosome fraction area was calculated for each profile by (1) manual definition of the fraction boundaries, (2) subtracting the lowest value in the profile from all points along the profile, and (3) manual integration using the trapezoid rule (see Figure S5B).

Intracellular amino acid quantitation

HEK293T cells in a 10 cm dish were washed twice with PBS on ice. Ice cold HPLC-grade 80:20 MeOH:H_2O was added to cells to extract polar metabolites. After vortexing, 80% methanol extracts were dried under vacuum and resuspended in water for analysis on an Agilent 6460 LC-MS/MS.

tRNA charging analysis

tRNA charging analysis was performed according to (Varshney et al., 1991) with the following modifications (see Figures 2, S2, and S4). 75% confluent cells in a 10 or 6 cm plate were washed once in PBS and flash frozen. Cells were scraped into ice cold 500 μL AE buffer (0.3 M NaOAc pH 4.5, 10 mM EDTA) on plates and added to 500 μL ice cold acid-saturated phenol:chloroform pH 4.5. Extractions were vortexed for 10 min, rested on ice for 3 min, and spun for 10 min at 20,000× *g* at 4°C. Aqueous supernatant was precipitated and resuspended in 10 mM NaOAc pH 4.5, 1 mM EDTA. To mark electrophoretic mobility of uncharged tRNA, RNA was deacylated in 100 mM Tris pH 9 at 37°C for 30 min, following by quenching with addition of an equal volume of 50 mM NaOAc, 100 mM NaCl and precipitation.

For acid urea gel electrophoresis, 500 ng–1 μg RNA and deacylated control in 0.1 M NaOAc pH 4.5, 8 M urea, 0.05% bromphenol blue, and 0.05% xylene cyanol were electrophoresed on a 0.4 mm 6.5% polyacrylamide gel (SequaGel) with 8M urea in 0.1M NaOAc pH 4.5 at 450V and 4°C for 18-20 hr. The gel region between the loading dye bands was excised and transferred according to "Northern blotting" section. Absolute charging level was calculated by dividing the intensity of the charged band(s) by the sum of all band intensities (quantified using ImageJ).

Probes for Northern blotting were designed to hybridize uniquely to tRNA isoacceptors, where possible, or isodecoders after alignment of all arginine and leucine tRNAs. All probes were validated for specificity by Northern blotting against *in vitro* transcribed target tRNAs and candidates for cross-hybridization identified by a genomic tRNA BLAST. We were not able to find uniquely hybridizing probes for $tRNA^{Leu}_{AAG}$ and $tRNA^{Leu}_{UAG}$ as these isoacceptor gene families have a great degree of sequence homology; however, the major species detected for these probes is the indicated tRNA (data not shown). We also note that two charged and uncharged species of $tRNA^{Arg}_{ACG}$ are detected (see Figures S2A and S2C), possibly due to covalent modification of this tRNA.

Western and dot-blotting

75% confluent cells in a 10 cm plate were lysed by scraping and pooling in 300 μL of 50 mM HEPES pH 7.4, 40 mM NaCl, 2 mM EDTA, 1 mM sodium orthovanadate, 10 mM sodium glycerophosphate, 10 mM sodium pyrophosphate, 50 mM sodium fluoride, 1% Triton X-100. After 10 min at 4°C, the insoluble fraction was cleared by centrifugation for 10 min at 4°C and 20,000 *g*. Lysate was electrophoresed in 1X Laemmli buffer on a 4%–20% Tris-glycine gel (Novex). Gels were transferred to 0.45 μm nitrocellulose in Towbin buffer with 20% methanol and 0.06% SDS using a semi-dry transfer system (Bio-Rad Trans-Blot SD) run at 15–20V for 1 hr. Primary antibodies are listed in Key Resources Table and were used at 1:1000 final dilution. The primary antibody from rabbit against puromycin was used at 1:25,000. HRP-conjugated secondary antibodies were used at 1:5000. 5% BSA in TBST was used for all blocking and antibody solutions for phospho-antibody blots, and 5% milk in TBST was used for all others. SuperSignal West Femto Substrate was used for developing, and Restore Western Blot stripping buffer was used to strip blots.

To calculate a relative phosphorylation index for mTORC1 and GCN2 targets to evaluate kinase activity, phospho-protein band intensity was divided by total protein band intensity and normalized to the appropriate maximum, minimum, or untreated ratio (see individual figure legends). This normalized phosphorylation index was first calculated for each sample on one technical replicate blot and then averaged between blots from replicate experiments although similar results were obtained using different normalization methods.

For dot-blotting, 2 μL of lysate was spotted onto a dry 0.45 μm nitrocellulose membrane, allowed to dry for 15 min, and then blots were processed as described above for western blotting (see Figures 5 and S5).

Northern blotting

After electrophoresis, gels were rinsed thoroughly in 0.5X TBE and transferred to HyBond Nylon+ membrane in 0.5X TBE using a semi-dry transfer apparatus (Bio-Rad Transblot) at 3 mA/cm^2 for 1 hr. The blot was crosslinked using the Stratalinker "auto-crosslink" setting once on each side, prehybridized in PerfectHyb buffer for 1 hr at 64°C, and hybridized at 64°C with 5 pmol probe (listed in Key Resources Table). Probes were end-labeled with [γ-P^{32}]-ATP using T4 PNK and purified with G25 Sepharose columns (GE Healthcare Life Sciences). The blot was washed 2x in a low-stringency wash buffer (2X SSC, 0.1% SDS) and 1X in a high stringency wash buffer (0.5X SSC, 0.1% SDS) at 64°C, exposed to a Phosphor-Imaging screen for 12–24 hr, and imaged using a Typhoon scanner.

Flow cytometry

Cells were trypsinized from a 6- or 12-well plate, quenched with DMEM + 10% FBS, and cells were pelleted by centrifugation at 125 *g* for 5 min. Pellets were resuspended in 500 μL (for a 12-well plate well) to 1 mL (for a 6-well plate well) of PBS and the cell suspension was passed through a 0.35 μm nylon mesh strainer-top tube (Corning). 10,000–30,000 events were collected for all experiments. YFP fluorescence measurements were log-transformed and the mean and standard deviation of all events was calculated from the population (see Figures 6 and S6).

Puromycin incorporation assays

75% confluent cells in a 6 cm plate were limited for leucine or arginine or grown in nutrient rich conditions for the desired time, followed by addition of puromycin (Sigma-Aldrich, P8833) to the culture medium at 10 μg/mL for exactly 5 or 10 min at 37°C. Cells were then washed once in ice-cold PBS and flash frozen in liquid nitrogen. Western blots or dot blots were performed to quantify puromycin incorporation into nascent polypeptide chains. To quantify blots, the total puromycin signal is integrated from each lane or dot and normalized to the signal intensity of a loading control (see Figures 5 and S5).

Reverse transcription & qPCR

RNA was extracted from cells in a 6-well plate with a Quick-RNA Miniprep kit (Zymo). Reverse transcription using a dT-20 primer or gene-specific primers was performed using Superscript III. cDNA template was diluted in water and qPCR was performed in 10 μL reaction volumes in 96-well plates, using the PowerUp SYBR Green PCR master mix (Thermo Fisher Scientific). To calculate relative YFP reporter mRNA levels, the YFP C_t value from qPCR analysis in each condition was normalized to the GAPDH C_t value to find ΔC_t, and then to the ΔC_t for the normalization sample indicated in figure legend to find $\Delta\Delta C_t$, which was converted to a normalized mRNA level by taking $2^{-\Delta\Delta Ct}$ (see Figure S6D).

Cell viability assays

20,000 cells were seeded in individual wells of 96-well plates (1 plate per assay time point, 5 technical replicate wells per plate) in amino acid limitation medium or rich medium. At desired time points, CellTiterGlo assay was performed with the following modifications. Cells were lysed by adding 1 volume of CellTiterGlo reagent and then transferred to an opaque black 96-well plate for luminescence reading. Luminesence was measured immediately on a TopCount instrument (Perkin Elmer) at 30°C. All viability measurements were normalized to an initial reading for each well taken 1.5 hr after seeding adherent cells (see Figure S6I).

QUANTIFICATION AND STATISTICAL ANALYSIS

Databases utilized

A subset of unique canonical transcripts used for mapping aligned ribosome profiling sequencing reads was defined based on the Gencode v24 database annotation file (gencode.v24.annotation.gff3). For each gene, only transcripts annotated as both CCDS and the APPRIS principal splice isoform (Rodriguez et al., 2013) were included; of this subset, the transcript with the lowest CCDS number for each gene was selected to generate a unique set.

tRNA gene numbers (see Figure S1K) were obtained from the genomic tRNA database (Chan and Lowe, 2016).

Ribosome profiling data analysis

Analysis was performed using R and Bash programming languages. For analysis code and more details see https://github.com/rasilab/adarnell_2018. The polyA tail was trimmed from 50 nt single-end raw sequencing reads using cutadapt (Martin, 2011) with a minimum length cutoff of 13 nt. A subtractive alignment was performed against ribosomal RNA using bowtie (Langmead et al., 2009), and the remaining reads were aligned to the transcriptome using rsem and bowtie (Li and Dewey, 2011). To calculate the pre-processing statistics and assess library quality (see Figures S1E–S1G), we used 3′ trimming of 12 nt for reads $\leq$ 32 nt and 13 nt trimming for reads > 32 nt to demonstrate 3 nt periodicity. For the rest of the analyses, as we were interested in the overall increase in ribosome density at codons and frame information was not required, we trimmed 12 nt from both sides to smooth our ribosome density profiles as previously described (Oh et al., 2011; Subramaniam et al., 2014). To calculate read counts for each transcript, each transcript position aligning to the trimmed read was assigned a count of the inverse value of the trimmed read length. The DESeq2 package was used to normalize each sample and then calculate gene fold changes (see Figures 3C and 3D) (Love et al., 2014).

To calculate the average ribosome density around each codon, only transcripts with a minimum average read density of 1 read per codon were considered. Reads at each transcript position were first normalized to the mean read count for that transcript. For each codon, the average read coverage was found for each position in a 150 nt window on either side of all occurrences of that codon. To calculate the change in average ribosome density around each codon upon amino acid limitation (see for example Figure 1B), the average ribosome density at each position in the 150 nt window around the codon in the rich condition was subtracted from that in an amino acid limited condition. To calculate the summed ribosome density at each codon (see for example Figure 1A), this 300 nt average ribosome density vector for each codon was summed.

Estimation of usage bias for pause-site arginine codons and GO analysis

We employed a binomial probability distribution to estimate the probability, for each gene, of having the observed number of CGC and CGU codons given the genome-wide average arginine codon usage frequencies (see Figure S1J). To avoid skew due to local GC bias in our analysis, we only considered sets of pause-site or non-pause-site arginine codons with equivalent GC content (CGC/CGU versus CGA/CGG, respectively; "CGN codons"). We calculated the average expected number of pause-site codons for each gene as the mean of a theoretical binomial probability distribution (μ); n*p, where n is the total number of arginine codons and p is the average frequency of stall sites relative to other CGN codons (p = 0.46). We calculated the standard deviation of that theoretical binomial probability distribution (σ) for each gene as the square root of n*p*(1-p). To then calculate a Z-score, we subtracted μ from the observed number of pause-site codons in that gene, and normalized by σ. When ranked, the resulting Z-scores range from -4.7 to 8.4 and represent bias toward (high scores) or against (low scores) the use of pause-site arginine codons to encode arginine in each gene (see Figure S6G).

Gene ontology (GO) analysis to detect enrichment for GO terms in genes with biased usage of pause-site arginine codons was performed in R using the topGO library (Alexa and Rahnenfuhrer, 2016). GO terms with a false-discovery rate adjusted p value of < 0.05 were visualized using REVIGO (Supek et al., 2011) (see Figure S6H).

Statistics

For all experiments, technical replicates refer to the repetition an entire experiment with a separate dish of cells split off from the same parental cell line (i.e., produced from the same lentiviral transduction or CRISPR editing process). Unless otherwise indicated in figure legends, three replicates were performed.

To assess whether summed differences in ribosome density at arginine and leucine codons correlated significantly with measures of codon usage frequency (Figures 1D, S1J, and S1M), cognate tRNA copy number (Figures 1E, S1K, and S1N), or cognate tRNA charging loss (Figure 2C) upon amino acid limitation, we performed a Spearman's rank-order correlation analysis. For this test, we considered $p < 0.05$ to indicate a significant correlation between the variables compared.

To assess whether the expression of mTORC1 or GCN2 target genes was significantly different between arginine and leucine limitation, we used a two-sided Wilcoxon signed rank test with continuity correction. For this test, the null hypothesis was that the median difference (μ) in the $\log_2$ fold change for each target between arginine and leucine limitation was equal to zero, and we considered $p < 0.05$ to indicate a significant differential mTORC1 or GCN2 response to arginine versus leucine limitation (Figures 3 and S3).

Fisher's exact test was used to determine significance in enrichment of GO terms in genes with the highest and lowest 5% of Z-scores (Figure S6G and S6H). GO terms with a false-discovery rate adjusted p value of < 0.05 were considered significantly enriched in genes with the strongest bias against (low Z-scores) or toward (high Z-scores) arginine pause-site codon usage.

DATA AND SOFTWARE AVAILABILITY

Full code and detailed instructions for generating the final figures in our paper starting from raw sequencing data are provided as a README.md file, interactive Jupyter notebooks, and static HTML files in the following Github repository (https://github.com/rasilab/adarnell_2018). The accession number for the raw and processed high throughput sequencing data reported in this paper is GEO: GSE113751.

Molecular Cell, Volume *71*

Supplemental Information

Translational Control through Differential Ribosome Pausing during Amino Acid Limitation in Mammalian Cells

Alicia M. Darnell, Arvind R. Subramaniam, and Erin K. O'Shea

Fig. S1, related to Fig. 1

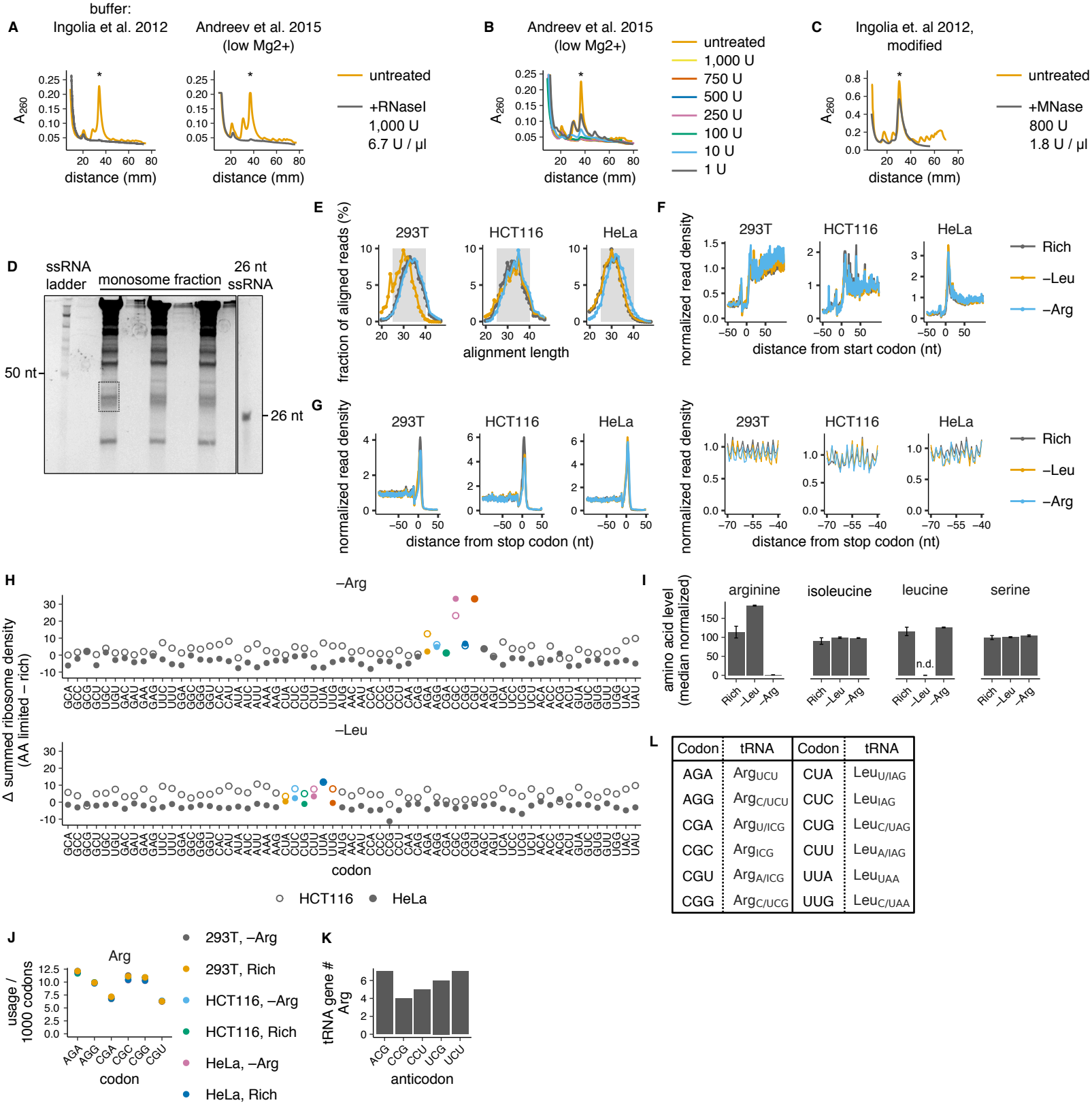

Codon	tRNA	Codon	tRNA
AGA	Arg_{UCU}	CUA	$Leu_{U/IAG}$
AGG	$Arg_{C/UCU}$	CUC	Leu_{IAG}
CGA	$Arg_{U/ICG}$	CUG	$Leu_{C/UAG}$
CGC	Arg_{ICG}	CUU	$Leu_{A/IAG}$
CGU	$Arg_{A/ICG}$	UUA	Leu_{UAA}
CGG	$Arg_{C/UCG}$	UUG	$Leu_{C/UAA}$

Figure S1

Codon-specific ribosome pausing emerges during limitation for arginine, but not leucine. (**A-C**) HEK293T cell polysome digestion into monosomes with varying amounts of RNaseI (B) in buffers with varying Mg^{2+} concentrations (A), or with MNase (C), was assessed by sucrose density gradient fractionation. (* = monosome fraction). (**D**) Representative size selection gel for RNA footprint extraction for library preparation. Box indicates the region excised. (**E-G**) Aligned read length distribution (E) and genome-wide read density profiles around annotated start (F) and stop codons (G) for data in Fig. 1A-C & S1H. After 3' end trimming, normalized read density is calculated as described in Fig. 1A & Methods. A region of the read density profile in G is magnified in a second (right) panel. (**H**) Overlaid summed changes in codon-specific ribosome density for HCT116 and HeLa cells following 3 hours of leucine or arginine limitation, calculated as described in Fig. 1A & Methods. Arg and Leu codons are colored according to the legend in Fig. 1. (**I**) Intracellular arginine, isoleucine, leucine, and serine levels in HEK293T cells following limitation for leucine or arginine for 3 hours or growth in rich medium. Error bars represent the standard error of the mean from three technical replicate measurements. Intracellular leucine level was below the detection limit (n.d.) upon its limitation. (**J**) Usage frequencies for Arg codons in the transcriptome in HEK293T, HCT116, and HeLa cells following 3 hours of limitation for arginine or growth in rich medium. (**K**) Genomic copy number of Arg isoacceptor tRNAs (Chan and Lowe, 2016). (**L**) Arg and Leu codons matched with their cognate tRNA(s). Decoding by multiple tRNAs is indicated with a slash, I = inosine.

Fig. S2, related to Fig. 2

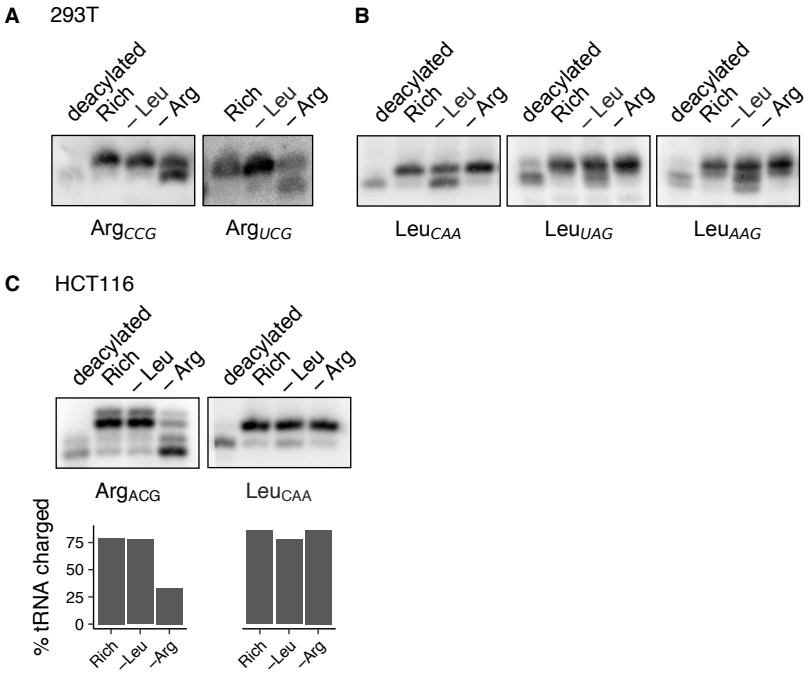

Selective loss of tRNA charging during arginine limitation. (**A-C**) Representative northern blots for determination of Arg and Leu tRNA charging levels (as shown in Fig. 2A,B) in HEK293T (A,B) cells or HCT116 cells (C) following 3 hours of limitation for leucine or arginine or growth in rich medium. A control deacylated total RNA sample is used to identify uncharged tRNA species. tRNA probe is indicated below each blot (see Methods for details of blot interpretation, quantification, and probe design).

Fig. S3, related to Fig. 3

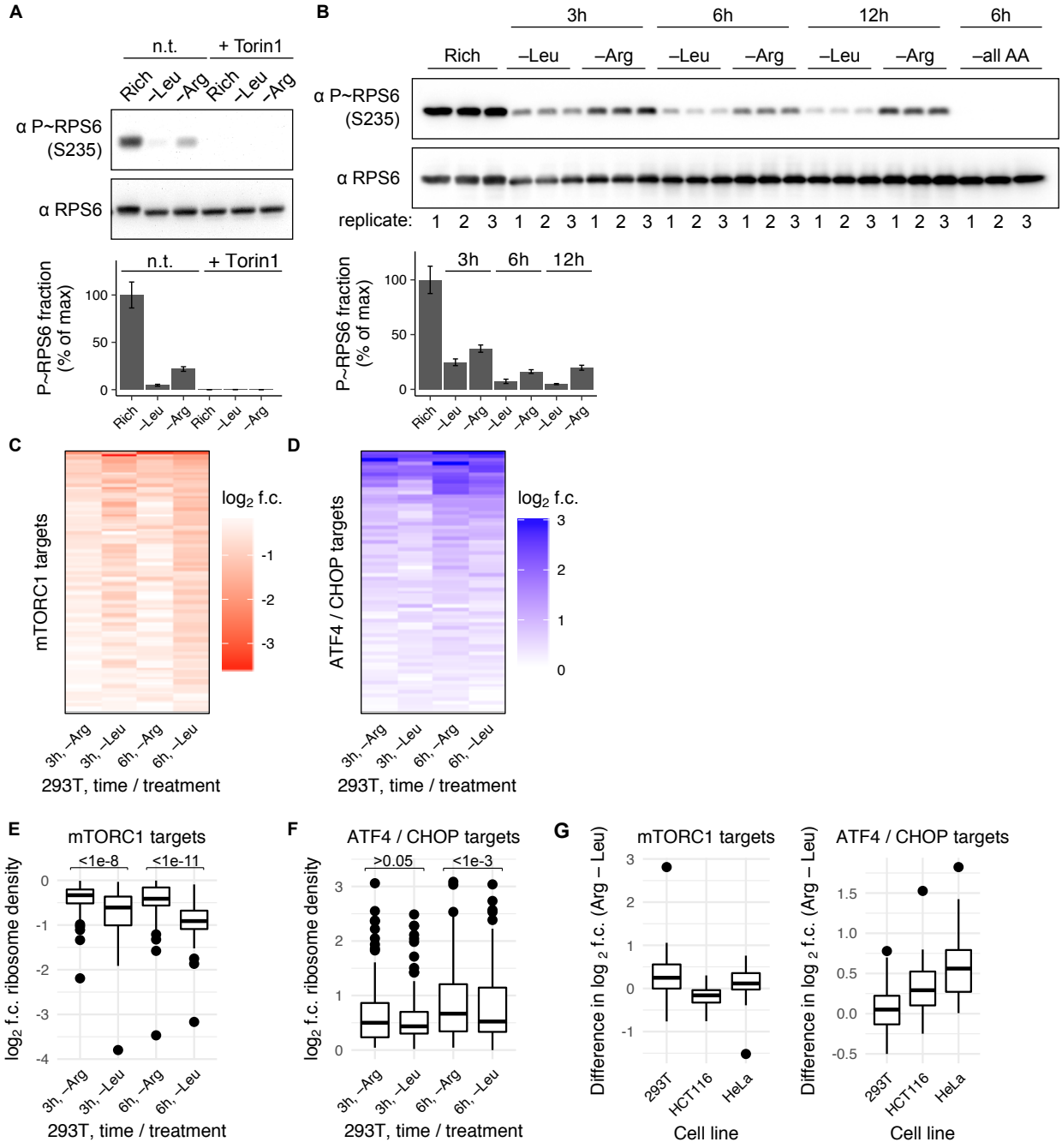

Differential mTORC1 and GCN2 responses to arginine and leucine limitation. (**A,B**) Representative western blots for phosphorylated and total levels of the S6K target, RPS6, in HEK293T cells after growth in rich medium or limitation for leucine or arginine for 3 hours + / - 250 nM Torin1 (A) or limitation for leucine or arginine for 3, 6 or 12 hours, or for all amino acids for 6 hours (B). Bar graphs show the fraction of protein that is phosphorylated in each condition, relative to rich medium; error bars represent the standard error of the mean from three technical replicate experiments. (**C,D**) Heatmap of $\log_2$ fold-changes (f.c.) in ribosome density for mRNA targets of mTORC1 inhibition (Hsieh et al., 2012) (C) or GCN2 activation via ATF4/CHOP (Han et al., 2013) (D) following 3 or 6 hours of leucine or arginine limitation, relative to rich medium, in HEK293T cells. Only targets with a $\log_2$ fold change of < 0, for mTORC1 targets, or > 0, for ATF4/CHOP targets, were considered. At 3 versus 6 hours, 43/73 (59%) versus 47/73 (64%) of mTORC1 targets (C), and 67/87 (77%) versus 77/87 (89%) of ATF4/CHOP targets (D) had higher ribosome density upon arginine than leucine limitation, respectively. (**E,F**) Box plot of the $\log_2$ fold change for each mTORC1 (E) or GCN2 (F) target upon amino acid limitation (as shown in C,D). A two-sided Wilcoxon signed rank test was performed with $\mu = 0$; the resulting p-value is shown for each comparison (see Methods for details). At 3 hours versus 6 hours, mTORC1 activity was 1.3- versus 1.4-fold higher (E), and GCN2 activity was 1- versus 1.1-fold higher, during arginine than leucine limitation, respectively (F). (**G**) Box plot of the difference in the $\log_2$ fold change between each mTORC1 or GCN2 target following 3 hours of limitation for arginine versus leucine in HEK293T, HCT116, and HeLa cells.

Fig. S4, related to Fig. 4

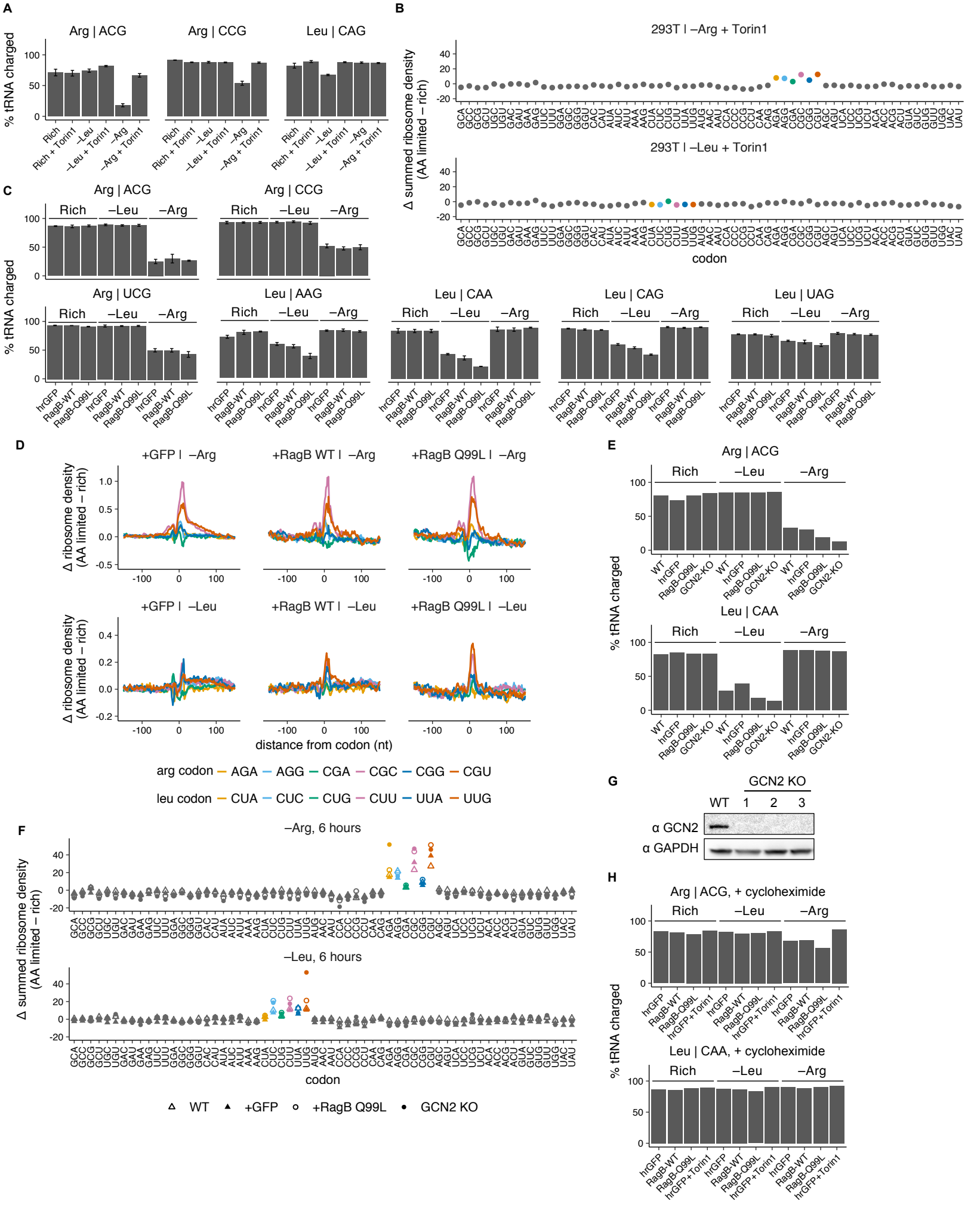

Figure S4

Signaling through the mTORC1 and GCN2 pathways regulates the magnitude of ribosome pausing during amino acid limitation. (**A**) tRNA charging levels for 2 Arg tRNAs and 1 Leu tRNA in HEK293T cells following 3 hours of leucine or arginine limitation or growth in rich medium, + / - 250 nM Torin1 (calculated as described in Methods). Error bars represent the standard error of the mean from three technical replicate experiments. (**B**) Summed changes in codon-specific ribosome density in the hrGFP cell line following 3 hours of limitation for leucine or arginine with 250 nM Torin1, relative to rich medium. Arg and Leu codons are colored according to the legend in D. (**C**) tRNA charging levels for 3 Arg and 4 Leu tRNAs in the hrGFP, RagB-WT, or RagB-Q99L cell lines following limitation for leucine or arginine for 3 hours or growth in rich medium (calculated as described in Methods). Error bars represent the standard error of the mean from three technical replicate experiments. (**D**) Changes in codon-specific ribosome density for the hrGFP, RagB-WT, and RagB-Q99L cell lines following limitation for leucine or arginine for 3 hours, relative to rich medium. (**E**) tRNA charging levels for 1 Arg and 1 Leu tRNA in the WT, hrGFP, RagB-Q99L, or GCN2 KO (see G) cell lines following limitation for leucine or arginine for 6 hours or growth in rich medium. (**F**) Overlaid summed changes in codon-specific ribosome density for the WT, hrGFP, RagB-Q99L, and GCN2 KO cell lines following 6 hours of leucine or arginine limitation, relative to rich medium. Arg and Leu codons are colored according to the legend in D. (**G**) Western blots for GCN2 and GAPDH proteins in HEK293T and 3 clonal replicate GCN2 KO cell lines. (**H**) tRNA charging levels for 1 Arg and 1 Leu tRNA in the hrGFP cell line + / - 250 nM Torin1, the RagB-WT, and the RagB-Q99L cell lines after exposure for <1 minute to 100 μg/mL cycloheximide in ice-cold PBS following limitation for leucine or arginine for 3 hours or growth in rich medium.

Fig. S5, related to Fig. 5

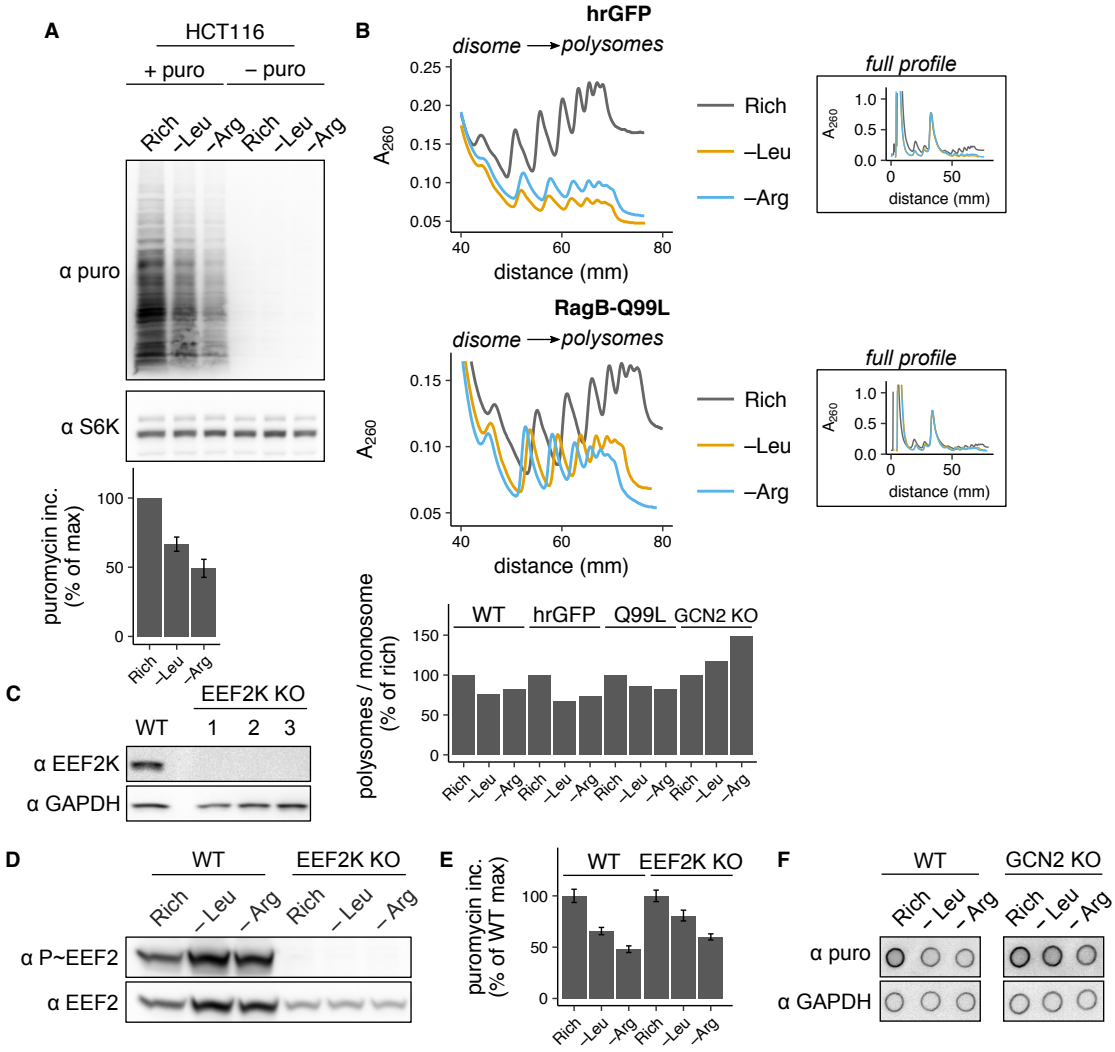

Ribosome pausing reduces global protein synthesis rate during amino acid limitation. (**A**) Representative western blots for puromycin and S6K in HCT116 cells after (+ puro) or without (– puro) a pulse of 10 μg/mL puromycin following 3 hours of leucine or arginine limitation, treatment with 250 nM Torin1, or growth in rich medium. Bar graph shows puromycin incorporation relative to rich medium (calculated as described in Methods); error bars represent the standard error of the mean from three technical replicate experiments. (**B**) Polysome profiles from the hrGFP and RagB-Q99L cell lines following 6 hours of leucine or arginine limitation or growth in rich medium. The main plot shows overlaid polysome profiles from the disome (2 ribosome) peak to the end of the polysomes, the inset plots show the entire profile. Bar graph shows the area in the polysome to monosome fraction, relative to that in rich medium (calculated as described in Methods). (**C**) Representative western blots for EEF2K and GAPDH in HEK293T and 3 clonal replicate EEF2K KO cell lines. (**D**) Western blots for phosphorylated and total EEF2 in WT and EEF2K KO cell lines following 3 hours of growth in rich medium, leucine limitation, or arginine limitation. (**E**) Puromycin incorporation in the WT (same data as Fig. 5D) or EEF2K KO cell lines following 3 hours of leucine or arginine limitation, relative to rich medium. Error bars represent the standard error of the mean for three technical replicate measurements. (**F**) Representative dot blots for puromycin and GAPDH in WT cells and the GCN2 KO cell line following 3 hours of leucine or arginine limitation or growth in rich medium.

Fig. S6, related to Fig. 6

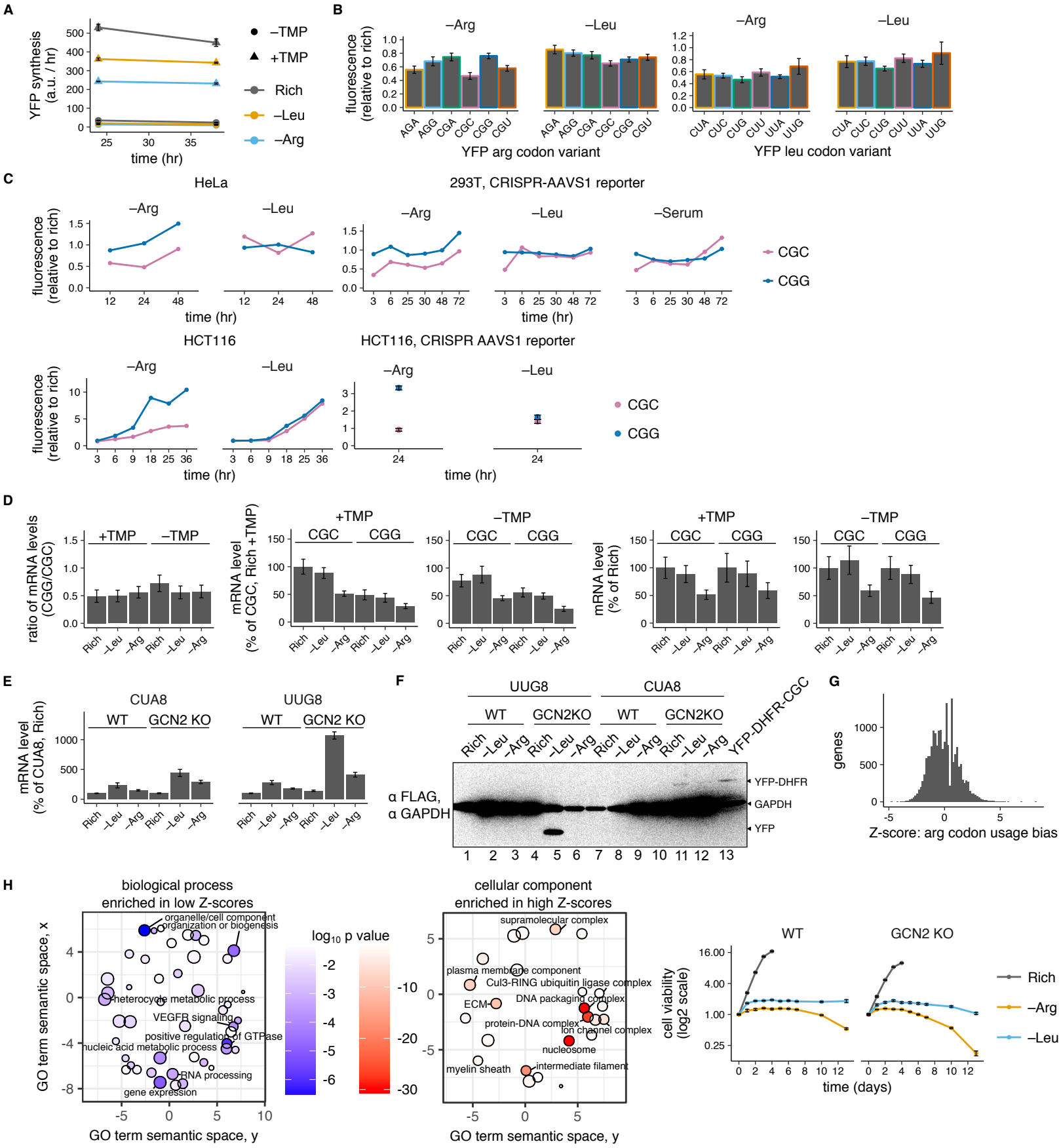

Figure S6

Ribosome pausing reduces protein expression from reporter mRNAs and induces premature termination of translation. (**A-C**) YFP codon variant reporter fluorescence measurements across multiple time points, cell lines, and reporter constructs (see Methods for details). Error bars represent the standard error of the mean from three technical replicate experiments. (**A**) Mean increase in YFP fluorescence per hour, + / - 10 μM TMP in HEK293T cells stably expressing the YFP-CGC reporter, following 24 or 38 hours of leucine or arginine limitation or growth in rich medium. (**B**) Mean YFP fluorescence in the HEK293T cells stably expressing the leucine or arginine YFP codon variant reporters following limitation for leucine or arginine with 10 μM trimethoprim for 24 hours, relative to rich medium +TMP. Arg and Leu codons are colored according to the legend in Fig. 6. (**C**) Mean YFP fluorescence in the HCT116, HeLa, and HEK293T cell lines stably expressing the YFP-CGC and -CGG reporters, following limitation for arginine, leucine or serum +TMP for 12, 24, or 48 hours, relative to rich medium +TMP. (**D**) YFP-CGC and -CGG CRISPR-AAVS1 reporter mRNA levels in HEK293T cells following 24 hours of limitation for leucine or arginine + / - TMP (calculated as described in Methods). From the left to right panel, the data is plotted 1) as the ratio of the YFP-CGG variant to the YFP-CGC variant for each condition, 2) normalized to the rich condition for the YFP-CGC reporter, 3) normalized to the rich condition for each YFP variant separately. Error bars represent the standard error of the mean for three technical replicate experiments. (**E**) CUA8 and UUG8 premature termination YFP reporter mRNA levels in the WT and GCN2 KO cell lines following 48 hours of limitation for leucine or arginine –TMP, relative to rich medium –TMP (see Methods section for details of calculation). Error bars represent the standard error of the mean for three technical replicate experiments. (**F**) Overexpressed blot image from Fig. 6I, for FLAG and GAPDH in the WT or GCN2 KO cell lines stably expressing the UUG8 or CUA8 reporters after growth in rich medium or 48 hours of leucine or arginine limitation. (**G**) Distribution of Z-scores reflecting pause-site arginine codon usage bias in coding sequences (see Methods section for details of calculation). (**H**) Biological process (BP) or cellular component (CC) gene ontology (GO) categories enriched in genes with bias against (left plot) or in favor of (right plot) usage of pause-site codons to encode arginine; visualized using REVIGO (Supek et al., 2011). Each bubble represents a significantly enriched GO term; color represents $\log_{10}$ of the false-discovery rate adjusted p-value, and size scales with the number of genes for a term. (**I**) Cell viability in the HEK293T or GCN2 KO cell lines following 1 to 13 days of leucine or arginine limitation, or growth in rich medium, relative to day 0. Error bars represent the standard error of the mean from five technical replicate measurements. Both cell lines reached confluency in rich medium after 4 days.